ÉCOLE POLYTECHNIQUE
FÉDÉRALE DE LAUSANNE

CRPP

ERASMUS Project, 2005-2006

Improvement of Diamagnetic Measurement on the TCV (Tokamak à Configuration Variable)

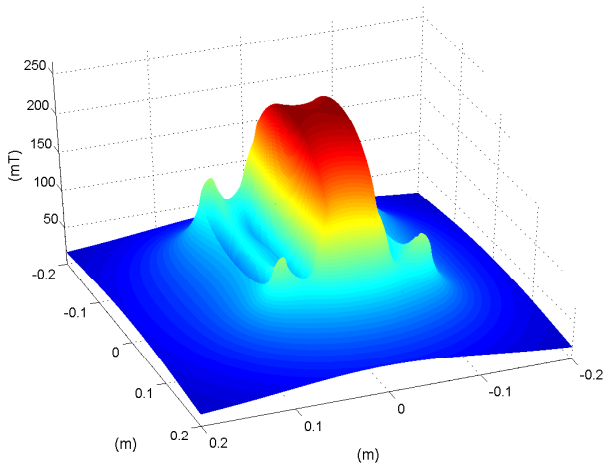

Robert Tye

Centre de Recherches en Physique des Plasmas (CRPP)

Under the direction of : Dr. Jean-Marc Moret

24th June 2006

Abstract

Fusion energy has the potential to provide us with an alternative to fossil fuels, which will eventually run out. One of the most promising designs for a fusion reactor is that of the Tokamak. The TCV (**T**okamak à **C**onfiguration **V**ariable) was designed to investigate the effects of plasma shape on stability, and as such allows for the creation of a variety of plasma shapes, up to three times higher than wide. Such a flexible plasma shape requires high precision magnetic measurements, and to this end the TCV is equipped with a wide range of magnetic probes and flux loops. One such system of flux loops is used to measure the plasma generated diamagnetic flux, which can then be used to calculate the plasma pressure. This system requires an accurate measurement of the current flowing in the tokamak's toroidal field coils, and to this end a system of probe coils was installed around the bars which supply this current. However, the installed system was designed on the assumption that the current would be evenly distributed between the bars, which is not the case during the ramping up and down of the current. The aim of this project, therefore, was to design a new system of probe coils which would see a flux that is independent of the distribution of current.

A model of the magnetic field produced by the current carrying bars was created using MATLAB, and rigorous testing found it to be suitable for the task. The magnetic field model was then used to create a model of the magnetic probe coils, which was also thoroughly tested. Using the probe coil model to model the original system, a linear relationship was found between the flux seen by the probe coil and the distribution of current between the bars. A solution to the problem was then found by modeling two subsystems of three probe coils each, such that the linear variation in the second was exactly opposite to that of the first. Adding these two subsystems together would then give a system which sees a flux that is independent of the distribution of current between the bars. This model was then used to design a new system of probe coils ready for construction.

Abstract

L'énergie de fusion représente une des principales alternatives à la diminution des réserves de pétrole. Un des systèmes les plus prometteurs permettant la fusion nucléaire est le Tokamak. Le Tokamak à Configuration Variable (TCV) a été conççu afin d'étudier les effets de la configuration du confinement du plasma sur la stabilité. Ce système permet ainsi une variété de formes de plasma allant jusqu'à créer un plasma trois fois plus haute que large. Cette flexibilité de configuration demande des mesures des champs magnétiques très précises, pour ce faire le TCV est doté d'un grand nombre de sondes magnétiques et de boucles à flux. Une de ces boucles à flux mesure le plasma engendré par le flux diamagnétique du plasma, qui permet par la suite le calcul de la pression du plasma. Ce système exige la mesure précise du courant circulant dans les bobines de champ toroidal du TCV. Cette précision est obtenue en installant une sonde, qui se présente sous la forme d'une bobine, autour des barres qui fournissent le courant. Ce système de mesure a été conçu et installé à partir de l'hypothèse d'une distribution uniforme de courant dans les barres. Ceci n'est cependant pas le cas lors du chargement et déchargement du courant. Le but de ce projet a ainsi été l'élaboration d'un nouveau système de sonde, qui serait uniquement sensible à un flux indépendant de la distribution de courant, permettant ainsi de se débarrasser du problème susmentionné.

On s'est alors d'abord intéresser à la modélisation du champ magnétique créé par les barres porteuses de courant. Ce modèle, conçu avec MATLAB, a subi une série de tests rigoureux qui se sont révélés satisfaisants. On a alors utilisé ces résultats pour la modélisation de la sonde en elle-même. Après des tests concluants le modèle de la sonde a été étendu au système original. On a alors remarqué une relation linéaire entre le flux reçu par la sonde et la distribution de courant dans les barres. La solution du problème a consisté à modéliser deux sous-systèmes de trois sondes chacun, de façon à ce que leurs variations linéaires soient opposées. L'addition de ces sous-systèmes nous donnerait alors un système total recevant un flux indépendant de la distribution de courant. Le modèle ainsi créé, a été ensuite utilisé pour la conception d'un nouveau système de sonde.

Contents

1 Introduction

1.1 Fusion

It is a fact that our supplies of fossil fuels will eventually run out, we may find more sources, new oil fields, new deposits of natural gas, but our supply will eventually run out. Our demand for energy, however, will only increase. We therefore need to find alternative sources of energy. Numerous possibilities exist to potentially fulfill our energy demands, such as solar power, wind power, wave power, hydroelectric power, nuclear fusion power, and, more controversially, nuclear fission power. All of these sources are renewable, they will never run out[1], and as such are all viable possibilities.

Fusion is the process by which two nuclei *fuse* together into one, larger, nucleus. To see where energy can be released through this process we shall look at the concept of nuclear binding energy. A bound nucleon, in its ground state, will sit at the bottom of the potential well of the nucleus, this potential well being caused by the strong nuclear force. The energy of the nucleon when sat in this potential well will be less than that of a free nucleon, thus the energy of a bound nucleus is lower than that of it's constituent particles. The binding energy of a nucleus is equal to the amount of energy which needs to be added to the nucleus in order to overcome all of the binding forces[2] and move the constituent particles (neutrons and protons) an infinite distance away from one another.

If the energy of the bound nucleus is lower than that of its constituent parts, then the rest mass of the nucleus must also be lower than the sum of the rest masses of the constituent protons and neutrons, due to Einstein's equation $E = mc^2$. This gives us a means of determining the binding energy of each nucleus by simply measuring its mass and comparing it to the total mass of the equivalent number of neutrons and protons. Figure 1 shows the average binding energy per nucleon for a range of different nuclei.

Lets say for example that we fuse a neutron and a proton together to form a deuteron (H^2), the mass of a neutron is $m_n = 1.675 \times 10^{-27} Kg$, the mass of a proton is $m_p = 1.6726 \times 10^{-27} Kg$, and the mass of a deuteron is $m_D = 3.3436 \times 10^{-27} Kg$, if you do the math then $m_p + m_n \neq m_D$, the total mass of an unbound neutron and proton is $3.965 \times 10^{-30} Kg$ more than the mass of the deuteron. Now this mass cannot have simply disappeared, but via Einstein's equation it could have been transformed into energy. This *lost* mass is equivalent to 2.224 MeV, so in the reaction $n + p \rightarrow D$ we would also have 2.224 MeV released, either as kinetic energy or radiation. This energy comes from the difference in binding energies. The neutron and proton when free have no binding energy, but when bound together into a nucleus they are sat in a potential well, which lowers their energy state, and the *lost* energy is released. Energy is freed by going from a weakly bound nucleus to a strongly bound nucleus and as can be seen in figure 1, the nucleus with the highest binding energy per nucleon, and thus the one most bound is the Iron (Fe^{56}) nucleus[3].

[1] Although fission power uses nuclear fuel rods, the amounts used are so small compared to the large amounts available that we may consider nuclear fission to be renewable. We may also consider nuclear fusion to be a renewable energy source, the two primary fusion fuels being deuterium which is abundant naturally in sea-water, and tritium which can be made from lithium.

[2] On the scale of a nucleus the largest force is the strong nuclear force, which dominates over coulomb repulsion, this is why nuclei can contain only positive charges and yet remain bound

[3] Iron stands as a turning point, for lighter nuclei we has fusion, and for heavier nuclei we have fission.

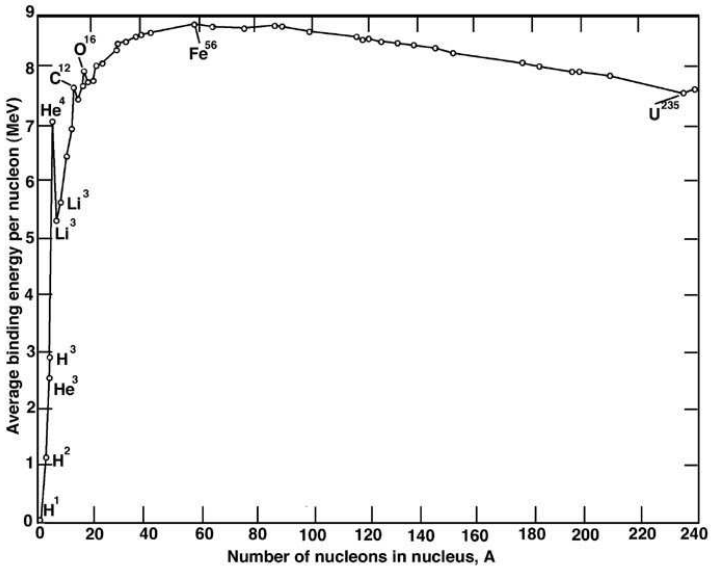

Figure 1: The binding energy per nucleon is simply the total binding energy for the nucleus divided by the number of nucleons in that nucleus.

Thus for nuclei with a greater mass than that of Iron, we can split the nuclei to release energy, this is the idea behind nuclear fission. Conversely, for nuclei with a lower mass than Iron we can release energy by the fusing of the smaller nuclei, this is the idea behind nuclear fusion. Several processes are proposed for a nuclear fusion reaction[4]:

1. $D + T \rightarrow He^4 + n + 17.58MeV$
2. $D + D \rightarrow T + H + 4.05MeV$
3. $D + D \rightarrow He^3 + n + 3.27MeV$

Where:

- D = Deuterium is a stable isotope of Hydrogen made up of 1 neutron and 1 proton
- T = Tritium is a radioactive isotope of Hydrogen containing 1 proton and 2 neutrons
- $1Mev = 1.6 \times 10^{-13} Joules$

Unfortunately these reactions do not just happen spontaneously (this is also a fortunate point, as otherwise all atoms would simply fuse together causing lots of problems). In order to fuse, the reactant nuclei must have enough kinetic energy to overcome the coulomb barrier and get close enough together such that the attractive strong nuclear force becomes dominant over the repulsive coulomb force. The D-T reaction (Reaction 1) has a break even temperature[5] of

[4]This is not an exhaustive list of all possible fusion reactions, but serves to demonstrate a few examples

[5]The break even temperature is the temperature at which the energy released by fusion balances the energy lost via radiation and the reaction becomes self sustaining.

4 KeV (around 45 million °C), whereas the D-D reaction (Reactions 2 & 3) has a break even temperature of 40 KeV (around 450 million °C) and to gain energy from the system requires even higher temperatures. The fact that the D-T cycle has a lower break even temperature and that it releases more energy makes it the more desirable reaction, however it still comes with several problems. Firstly, Tritium has a half life of 12.4 years, meaning it it is not found naturally in any significant quantities, and therefore must be bred in the reactor from lithium via one of the following processes:

$$n + Li^6 \rightarrow T + He^4$$
$$n + Li^7 \rightarrow T + He^4 + n$$

Furthermore, Lithium is less abundant than Deuterium, which occurs naturally in sea-water[6]. Another problem with the D-T reaction is that the majority of energy is released as kinetic energy in the form of fast neutrons. The only way to turn the kinetic energy of neutrons into useful energy such as electricity is to convert it into heat and then use a thermal cycle to turn it into electricity, which is not a particularly efficient process. Finally, the large number of neutrons released will also induce radioactivity in the reactor materials, causing a problem for safe disposal.

Each of the different fusion reactions come with their own set of problems, however the greatest problem lies in starting the reaction in the first place. The incredibly high temperatures involved mean that the fusion reaction cannot be contained within any material container, for two reasons. Firstly, as it would cause the container to melt, and secondly if the fusion reactants came into contact with the walls of the container then they would cool down and the fusion reaction would stop. We can however use the fact that at these very high temperatures the gas will be ionized, becoming a plasma, allowing us to use a magnetic confinement system such as a tokamak.

1.2 The Tokamak à Configuration Variable

1.2.1 Tokamaks

High temperature plasmas can be contained by exploiting the fact that a plasma is an ionised gas, made up of ions and electrons, and can therefore be contained by using powerful magnetic fields. A charged particle moving in a constant and uniform magnetic field will describe a helical path along the magnetic field lines[7], due to the Lorentz force $F = q\vec{v} \times \vec{B}$ (see figure 2). It can move freely along the field lines but cannot move across them, effectively confining it within a *magnetic bottle*. However, the particles can still escape from the ends off the magnetic field, but if the magnetic field is bent into the shape of a torus then there are no ends and the charged particles are effectively contained, this is the principle behind a Tokamak. The basic design of a tokamak consists of a *donut* or *torus* shaped vacuum chamber, into which a very low density gas (deuterium in the case of the TCV) is placed. The gas is then heated to a very

[6]The amount of deuterium contained in one litre of sea-water could release the same energy as roughly 300 litres of petrol

[7]Magnetic field lines represent the direction of the magnetic field, they are drawn close together to represent a strong magnetic field and further apart to represent a weaker magnetic field.

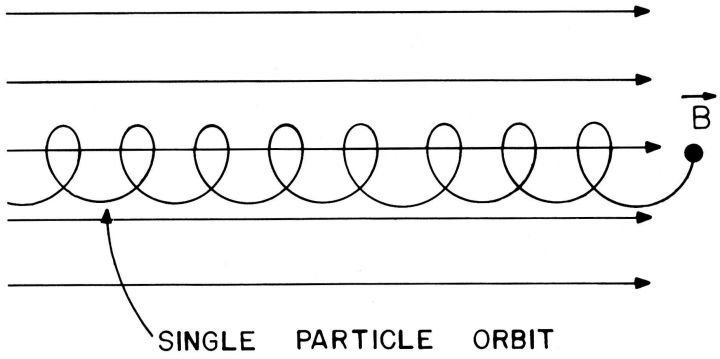

Figure 2: In a constant uniform magnetic field a charge particle can move freely along the field lines, describing a helical path, but cannot move across lines. Figure taken from [2], page 8.

high temperature, typically several hundred million degrees, causing it to ionise and become a plasma. The vacuum chamber is surrounded by various field coils which produce the magnetic field necessary to contain the extremely hot plasma, a basic schematic of a tokamak can be found in figure 3.

Bending the magnetic field, however, causes it to become inhomogeneous, stronger towards the center of the torus and weaker further out. This gradient in the $\vec{B}$ field causes the particles to drift towards the outside of the torus and eventually be lost. This movement can be averaged to zero by adding a poloidal field component (see figure 3 for a definition of poloidal and toroidal), giving an overall helical field. In this way the particles spiral around in the tokamak and the overall effect of drift is neutralised. The most common means of creating this poloidal field is to induce a current in the plasma[8] by using the plasma as the secondary turning of a transformer. Figure 3 shows the layout of a basic tokamak, the toroidal field is created by current carrying loops wrapped around the torus, and the poloidal field is caused by the plasma current. Various other processes can cause the plasma to escape from the magnetic confinement, such as particle collisions and plasma instabilities. In order to counter and control these effects it is important to have an accurate knowledge of the magnetic fields within the tokamak, and therefore to have accurate magnetic diagnostic systems.

1.2.2 The TCV

The **T**okamak à **C**onfiguration **V**ariable (**TCV**) started operation in November 1992, at CRPP (**C**entre de **R**echerches en **P**hysique des **P**lasmas), the main center of plasma physics research in Switzerland, based at EPF Lausanne. The aim of the TCV is to investigate the effect of plasma shape on confinement and stability. For this purpose the TCV provides a high flexibility in plasma shape, and allows plasma cross sections which are up to three times higher than they are wide. In order to control the shape of the plasma, a large number of poloidal field coils have been built into the TCV, along with the toroidal field coils these give a high degree of control over the shape of the magnetic field, and thus the plasma contained within. Figure 4 shows the

[8]Being a collection of charged particles a plasma can act as a conductor

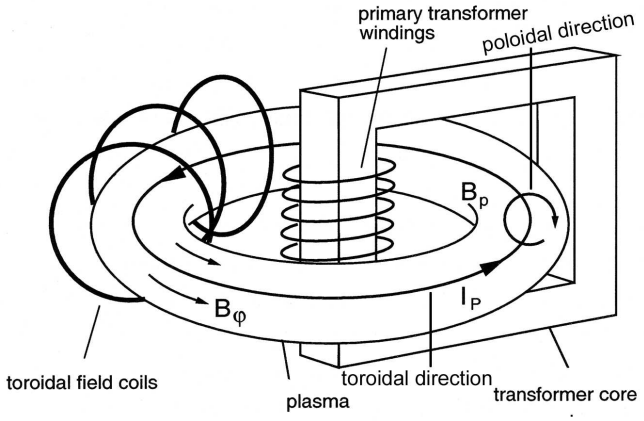

Figure 3: Basic schematic of a tokamak, showing the toroidal field coils which are wound around the torus and which produce the toroidal magnetic field, and the transformer used to induce the plasma current. For clarity the diagram also shows the toroidal and poloidal directions with respect to the tokamak. Figure taken from [5], page 2.

major parts of the TCV, while figure 5 shows some of the many varied plasma shapes which can be achieved. This high level of control over the magnetic field requires numerous feedback systems, placed both within and outside the tokamak. These systems need to be both accurate and fast in order to allow maximum control over the plasma.

1.3 Magnetic Systems and Diagnostics within the TCV

Having a high flexibility in the shape of the plasma requires numerous magnetic measurements which need to be both fast and precise. This section details some of the magnetic containment systems and magnetic diagnostics installed within the TCV. A poloidal cross section of the tokamak, detailing the location of all of the coils and parts outlined below can be found in figure 6.

1.3.1 The Ohmic Transformer, Poloidal Shaping, and Toroidal Field Coils

The plasma current in the TCV is induced using an air core transformer, where coils A - D (see figure 6) act as the primary turnings of the transformer, while the plasma itself acts as the secondary turning. The flexibility in the shape of the plasma is made possible by the large number of poloidal shaping coils, divided into two stacks (E & F) of eight coils each, one stack circling the outside of the tokamak, with the other running along the interior radius. The toroidal field, whose main function is to contain the plasma, is produced by 16 coils which surround all of the other coils and the vacuum vessel (see figure 4)

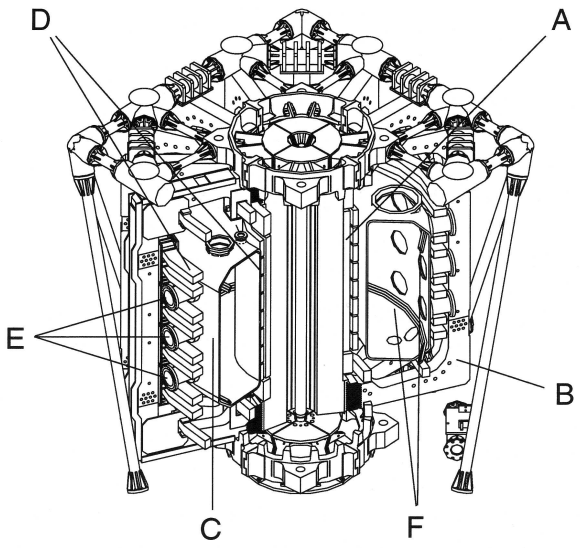

Figure 4: A schematic of the TCV, showing the ohmic transformer coils (A) which are used to induce the plasma current, the toroidal field coils (B), the vacuum vessel (C), the poloidal field coils (C) which are used to shape the plasma, the diagnostic ports (E), and the internal control coils (F). Figure taken from [5], page 10.

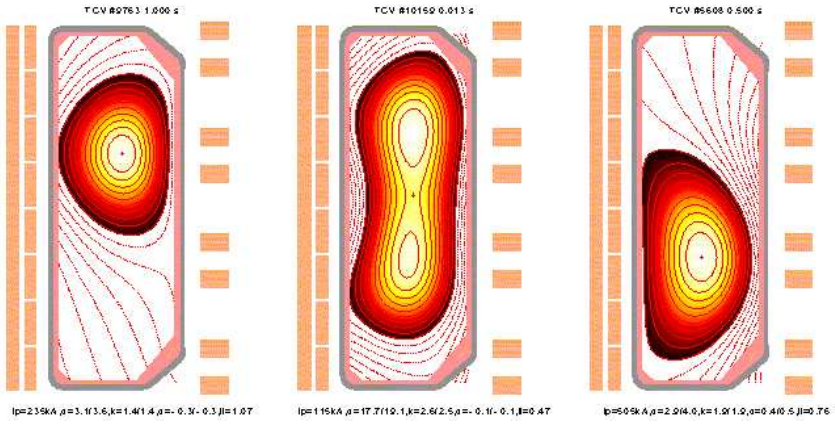

Figure 5: Some of the various plasma shapes which can be achieved within the TCV.

1.3.2 Magnetic Probes

There are four sets of 38 magnetic probes, separated toroidally by 90°. These coils are placed such that they can measure the poloidal component of the magnetic field, tangential to the vacuum vessel. The signals from these probe arrays are fed into the real time plasma shape and position control system. The signals from two opposite arrays can then be used to cancel any toroidal asymmetries in the plasma. There are also two further sets of these magnetic probes, placed at equal toroidal separation, one set of eight probes placed at the same poloidal position as probe 1, and a second set of sixteen probes placed at the same poloidal position as probe 20 (magnetic probe locations are marked with the corresponding number in figure 6). These probes are used for MHD (MagnetoHydroDynamic) mode analysis.

The probes are constructed from two layers of twenty turns of THERMOCOAX®[9] wound onto a molded ceramic core. They are then spring loaded onto brackets which sit behind the heat resistant graphite tiles. These tiles line the entire interior surface of the vacuum vessel, in order to protect the metal vessel from the hot plasma. The wires are continuous from the probes until outside, to reduce problems caused by multi-poles in the circuit.

1.3.3 Poloidal Flux Loops

Represented in figure 6 with 'x's, these poloidal flux loops run the circumference of the tokamak. The flux loops on the vacuum vessel are made from THERMOCOAX® in order to stand the high temperatures, while the flux loops on the poloidal coils are made from adhesive copper band. The fluxes from the different loops can be used to reconstruct the shape of the magnetic field and of the plasma, and are used in the real-time control of the plasma shape.

1.3.4 Using Diamagnetic Measurements to Calculate the Plasma Pressure

It is possible to calculate the normalised plasma pressure, or poloidal beta, β_p from the plasma generated diamagnetic flux, ϕ_p, using the following equation (from [7]):

$$\phi_p = \frac{\mu_0^2 I_p^2}{8\pi B_t}(1 - \beta_p) \tag{1}$$

The calculation requires highly precise measurements of ϕ_p over very small timescales (changes in the plasma pressure can occur over 1 to 100 ms in the TCV). Unfortunately the magnetic flux ϕ_p is mixed in with several other, much stronger, magnetic fluxes. There are three main sources of toroidal magnetic flux:

- The plasma generated diamagnetic flux, ϕ_p.
- The flux produced by the current, I_t, in the toroidal field coils.
- The flux produced by the current, I_v, induced in the walls of the vacuum vessel by mutual inductance with ϕ_p & I_t.

[9] A micro-coaxial cable, with a copper core and an Inconel shell.

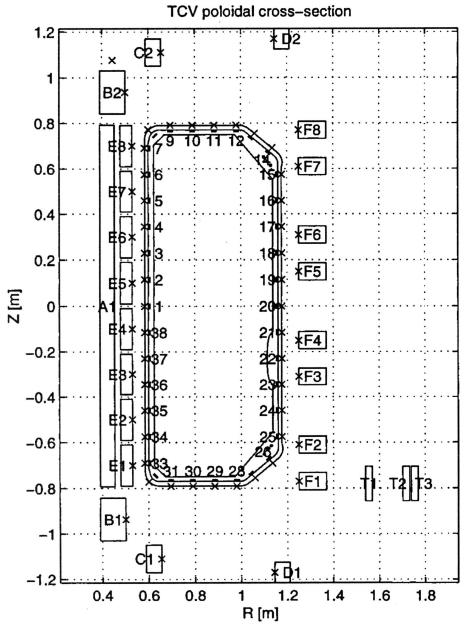

Figure 6: A poloidal cross section of the TCV, showing the ohmic transformer coils (A-D), the poloidal shaping coils (E-F), as well as the positions of the magnetic field probes (shown as a small bar next to a number), and the poloidal flux loops (marked with an x). Figure taken from [6], page 2334.

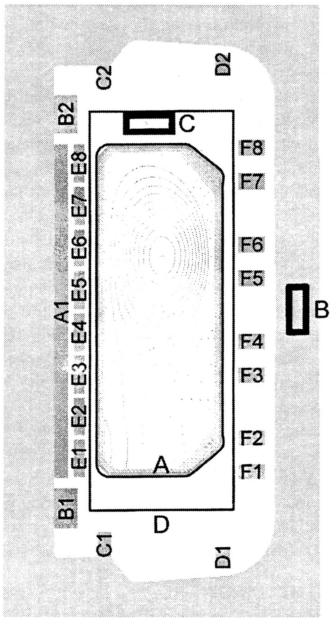

Figure 7: A poloidal cross section showing the single (A & D) and multi (B & C) turn loops used for diamagnetic measurements in the TCV. These loops can be used to find the toroidal magnetic flux from the plasma, ϕ_p, and subsequently the plasma pressure.Figure taken from [7], page 4635

It is possible to measure ϕ_p using a combination of flux loops, placed such that they see different combinations of the three fluxes. Figure 7 shows the position of these different flux loops, which see different fluxes as follows:

- Loop A is made of a single turn of mineral insulated coaxial wire wound directly onto the vacuum vessel, and is used to assess the vessel image currents.
- Loop C is and 80 turn coil, engraved onto a printed board, with an area such that it catches the same flux as loop D. Loop C is used to compensate for the flux from the toroidal field coils.
- Loop D is positioned to measure the total toroidal flux from the toroidal field coils, the plasma, and the vessel image currents.

The voltages measured by loops A, C, and D are given by the following equations in the Laplace domain[10]:

$$\begin{pmatrix} U_D \\ U_C \\ U_A \end{pmatrix} = \begin{pmatrix} s & sM_{Dt} & sM_{Dv} \\ 0 & sM_{Ct} & 0 \\ s & sM_{At} & sM_{Av} \end{pmatrix} \begin{pmatrix} \phi_p \\ I_t \\ I_v \end{pmatrix} \tag{2}$$

A linear combination of these voltages can, therefore, be found which could be used as an estimate for ϕ_p, the exact derivation of which adds little to the work done here, but can be found in [7].

What we are interested in in this project is loop C, looking at equation (2) we see that loop C should only see the flux from the toroidal field coils. However, if the loop is slightly misaligned, and not completely perpendicular to the toroidal field, then it will see other fluxes such as those from the poloidal field coils, causing an inaccurate measurement of the plasma pressure. Ideally we would like to place loop C such that it only sees the flux from the current in the toroidal field coils, and is not susceptible to the various other magnetic fields in and around the tokamak. If we look at the equation for the flux seen by loop C:

$$\phi_c = M_{Ct} I_t \tag{3}$$

we see that the flux is directly proportional to the current I_t, and M_{Ct} is just a constant, dependant upon the geometry and position of the coil with respect to the current I_t. It is therefore not important where we place loop C, as long as the flux passing through it is directly proportional to I_t. A solution would therefore be to place a system next to the bars which supply the current to the toroidal field coils (a cross section of which can be found in figure 10). This would allow us to place the loop away from the strong magnetic fields surrounding the tokamak. A possible system which would fulfil our requirements would be a Rogowsky coil.

1.3.5 The Rogowsky Coil

The basic form of a Rogowsky coil is a solenoid which has been deformed into a torus (see figure 8). The interesting part for us is that the flux which threads the windings of the coil is directly proportional to the current which passes through the major opening of the torus. If the turnings of the coil are evenly spaced then the flux ϕ can be written as (from [4]):

$$\phi = \frac{An\mu_0}{S} I = M_{RI} I \tag{4}$$

Where A is the area of an individual turn, S is the mean circumference of the torus, and n is the number of turns. This result is also independent of the major shape of the Rogowsky coil, as long as the shape is topographically equivalent to that of a torus. Equation (4) corresponds exactly with what we are looking for, therefore a suitable solution to our problem would be to simply place a Rogowsky coil around the current carrying bar.

[10] The Laplace transformation is given by:

$$f(s) = \lim_{a \to \infty} \int_0^a e^{-st} F(t) dt$$

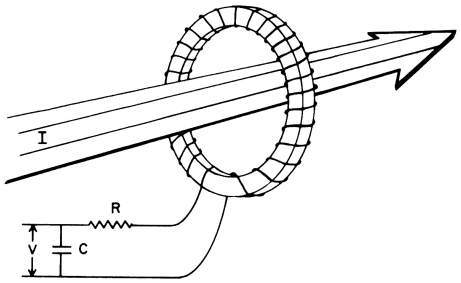

Figure 8: A Rogowsky coil, the flux seen by a rogowsky coil is directly proportional to the current, I, which passes through the major opening of the torus. Figure taken from [4], page 11.

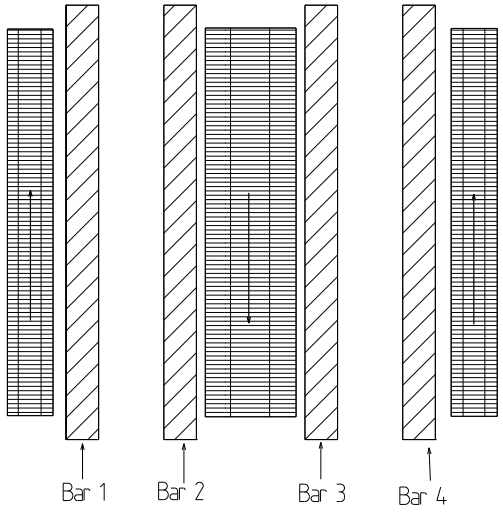

Figure 9: The current semi Rogowsky coil, the arrows represent the vector direction of the surface of the flux loops, and the coils are joined in series.

Unfortunately things are never simple, and this case is no exception. Due to the restricted space around the current carrying bars it is not possible to install a full Rogowsky coil. An attempt was made, however, at installing a semi-Rogowsky coil (see figure 9). The semi-Rogowsky system is made up of three probe coils, two identical coils placed one at each side of the arrangement of current carrying bars, and a central probe coil. The probe coils are connected in series, but in such a way that the central coil has a surface vector which is opposite to the outside coils. This basically represents two Rogowsky coils in series, one on the left, made up of the left hand coil and the central coil, and a second on the right made up of the central coil and the right hand coil.

The two left hand current carrying bars carry current out of the paper, towards the toroidal field coils, whereas the two right hand bars carry current into the paper, away from the toroidal field coils.[11] This is reflected in the way the probe coils are joined together, as the left-hand semi-Rogowsky will give a positive flux for clockwise magnetic fields, and a negative flux for anti-clockwise magnetic fields, and vice-versa for the right-hand semi-Rogowsky. Thus a current coming out of the page in the two left-hand bars will cause an anti-clockwise magnetic field, and thus a negative flux in the left-hand semi-rogowsky, and similarly the current going into the page in the two right-hand bars will cause a negative flux in the right-hand semi-rogowsky. So the total flux should be proportional to the negative of the total current, and should solve our problem.

There exists, however, a flaw in this system, it was designed under the assumption that the current would be evenly distributed within the pairs of current carrying bars, such that:

$$I_1 = I_2 = -I_3 = -I_4$$

[11]The two left hand bars are connected together, and the same for the two right hand bars

This is certainly the case when the current is steady, however during the ramping up and down of the current a magnetic field is produced, which acts against the current and changes its distribution within the bars. This exposes the ambiguity in the currently installed system, different distributions of the same current will give different fluxes, meaning the flux is no longer directly proportional to the current, and so a good calculation of the plasma pressure cannot be achieved.

It is the aim of this project, therefore, to design a new system which takes into account the possible uneven distribution of current within the bars. The new system should see a flux which is directly proportional to the current I_t, and be unaffected by external magnetic fields.

2 Modelling the Magnetic Field

In order to model a system which measures the magnetic field of the current carrying bars, it is first necessary to model the magnetic field itself. For purposes of clarity, Figure 10 shows the arrangement of the four bars, which we will refer to as bars 1-4. We shall assume a right-handed axis system, also shown in figure 10, where the $z - axis$ comes out of the page and represents the direction of positive current flow. The four bars in the system are each of rectangular cross section, and the sensors will be placed close enough to the bars that we can essentially view the bars as being infinitely long in the direction parallel to the $z - axis$. Treating the bars as being infinitely long removes any field distortions which may be caused by end effects The field can then be treated as non-varying along the $z - axis$, allowing the problem to be solved in 2D rather than 3D, which will save a lot of processor time. To further simplify the problem, it is assumed that current is distributed uniformly within each of the bars, however the current in each bar may be different. The linear nature of magnetic fields makes it possible for us to model the magnetic field of just one bar and then to add together the fields calculated for bars at different locations and with different currents.

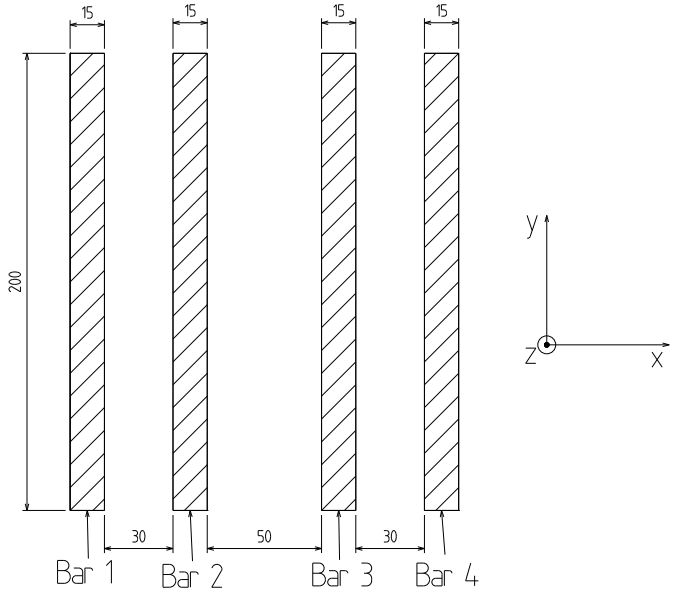

Figure 10: Left: Cross sectional diagram of the four current carrying bars (all dimensions are in mm). Right: Right handed set of axis in relation to the arrangement of bars, the positive $z - axis$ points out of the paper and represents the direction of positive current flow.

2.1 Deriving the Mathematical Representation of the Magnetic Field of a Current Carrying Bar

Let us start with the simplest possible model of a single bar, that being the model of a filamentary conductor. If we take a filamentary conductor of cross section ds, length $2l$, and carrying a

current of jds, then the magnetic potential, $d\vec{A}$, of the filament can be calculated using the *Biot-Savart* law (5):

$$d\vec{A} = \frac{\mu}{4\pi} jds \int_{-l}^{l} \frac{d\vec{l}}{r_{PQ}} \tag{5}$$

where μ is the magnetic permeability, $d\vec{l}$ is an infinitesimal element of the filament, and r_{PQ} is the distance between the infinitesimal element of the filament $d\vec{l}$ and the point at which we wish to measure the magnetic field. Since in our system we are working with straight conductors, we can define the current to be traveling in a direction parallel to the z axis, and so $d\vec{l}$ becomes dz, and similarly $d\vec{A}$ becomes dA_z. If we further define $r_{PQ} = \sqrt{r^2 + z^2}$ where $r^2 = x^2 + y^2$, then we can fully utilise the symmetries of the system and the *Biot-Savart* law is then represented by equation (6)

$$dA_z = \frac{\mu}{4\pi} jds \int_{-l}^{l} \frac{dz}{\sqrt{r^2 + z^2}} \tag{6}$$

which, by symmetry then becomes (7)

$$dA_z = \frac{\mu}{2\pi} jds \int_{0}^{l} \frac{dz}{\sqrt{r^2 + z^2}} \tag{7}$$

which we can then integrate (using $\int \frac{dz}{\sqrt{r^2+z^2}} = \ln\left(z + \sqrt{r^2 + z^2}\right)$) to get equation (8)

$$dA_z = -\frac{\mu}{2\pi} jds \left(\ln r - \ln\left(l + \sqrt{l^2 + r^2}\right)\right) \tag{8}$$

If we make the assumption that $l >> r$ then we finally arrive at an expression for the magnetic potential of a filamentary conductor (9)

$$dA_z = -\frac{\mu}{2\pi} j \left(\ln r - \ln 2l\right) ds \tag{9}$$

Of course the representation of the magnetic potential of a filament is useful, but not exactly what we were looking for. In order to represent a bar of finite height and width, the equation for the filamentary element must be integrated over the cross sectional area of the bar. In the case of a bar with height $2b$, width $2a$, and thus area $4ab$, centered at the origin of the xy plane (see Fig. 11 for a graphical representation), we must carry out the following integral (10)

$$A_z(x, y) = -\frac{\mu}{2\pi} \frac{I}{4ab} \int_{-a}^{a} \int_{-b}^{b} \ln\left(\sqrt{(x' - x)^2 + (y' - y)^2}\right) dx'dy' \tag{10}$$

The $\ln 2l$ term from equation (9) has been omitted in equation (10), the reason for this becomes obvious if we look at equations (11) and (12) which relate the magnetic intensity and the magnetic potential. As the $\ln 2l$ term is independent of r it will disappear in the partial differentials: $\frac{\partial A_z}{\partial y}$ and $\frac{\partial A_z}{\partial x}$, and thus will not affect the calculation of the magnetic intensity. Once we integrate equation (10) and arrive at a suitable formula for the magnetic potential created by the

current carrying bar, the following relations can be used to determine the magnetic intensities H_x & H_y[12]

$$H_x = \frac{1}{\mu}\frac{\partial A_z}{\partial y} \tag{11}$$

$$H_y = -\frac{1}{\mu}\frac{\partial A_z}{\partial x} \tag{12}$$

After much integration and rearrangement, we arrive at the following set of equations (Equations 13 & 14) to describe the magnetic field created by a long, straight, current carrying bar (see figure 11 for a graphical representation of the variables a, b, r_1, r_2, r_3, r_4, ϕ_1, ϕ_2, ϕ_3, and ϕ_4).

$$H_x(x,y) = -\frac{I}{8\pi ab}\left[(y+b)(\phi_1-\phi_2) - (y-b)(\phi_4-\phi_3) + (x+a)\ln\frac{r_2}{r_3} - (x-a)\ln\frac{r_1}{r_4}\right] \tag{13}$$

$$H_y(x,y) = \frac{I}{8\pi ab}\left[(x+a)(\phi_2-\phi_3) - (x-a)(\phi_1-\phi_4) + (y+b)\ln\frac{r_2}{r_1} - (y-b)\ln\frac{r_3}{r_4}\right] \tag{14}$$

$$r_1 = \sqrt{(x-a)^2+(y+b)^2} \qquad \phi_1 = \arctan\frac{y+b}{x-a}$$

$$r_2 = \sqrt{(x+a)^2+(y+b)^2} \qquad \phi_2 = \arctan\frac{y+b}{x+a}$$

$$r_3 = \sqrt{(x+a)^2+(y-b)^2} \qquad \phi_3 = \arctan\frac{y-b}{x+a}$$

$$r_4 = \sqrt{(x-a)^2+(y-b)^2} \qquad \phi_4 = \arctan\frac{y-b}{x-a}$$

A lot of steps in the derivation of equations 13 & 14 from equation 10 have been omitted as they do not add anything significant to the work done here, however a more complete treatment can be found in pages 107-110 of [1].

2.2 Creating a Computer Model of the Magnetic Field of a Single Current Carrying Bar

Having arrived at a suitable set of equations to describe the magnetic fields created by the current carrying bars, we can now create a mathematical computer model of the field. All models within this paper have been created using MATLAB, a widely distributed mathematical software package. The first step is to create a simple model for one bar, once we have this basic model it can be replicated at different positions to create our arrangement of bars.

In order to test the validity of the proposed model, let us first take a look at a few simple examples. In figure 12 we see the magnetic field calculated for a bar of cross section $20cm$ by

[12]Confusion is often caused when it comes to naming the values H and B, related by $B = \mu H$. In order to avoid confusion, in this paper H will always be referred to as the magnetic intensity and B will always be referred to as the magnetic field.

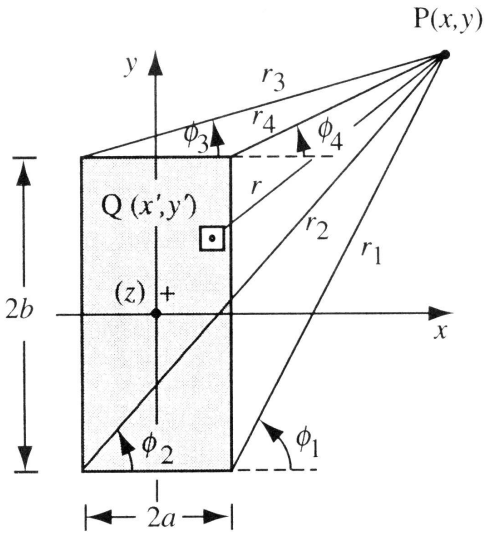

Figure 11: Graphical representation of the variables a, b, r_1, r_2, r_3, r_4, ϕ_1, ϕ_2, ϕ_3, and ϕ_4 used in equations (13) & (14). Figure taken from [1], page 108.

.

$20cm$ carrying a current of $100A$ (coming out of the page towards the reader). On the left is a quiver plot of the field, with the length and direction of the arrows representing the strength and direction of the field at each point, while on the right is a coloured contour plot representing the field strength. The blue square in the centre represents the position and size of the bar. From a purely visual standpoint this model corresponds well with what we would expect. The anti-clockwise direction of the magnetic field is what we would expect from Maxwell's equations for a current coming out of the paper.[13]The calculated field strength also corresponds well with what we would expect to see, decreasing as we move away from the bar and as we move towards the centre of the bar. [14]

As we move further and further from the bar, the calculated field should theoretically tend towards that of an infinite current carrying filament, described by equations (15) & (16).

$$B_x = -\frac{\mu I}{2\pi}\frac{y}{x^2+y^2} \tag{15}$$

$$B_y = \frac{\mu I}{2\pi}\frac{x}{x^2+y^2} \tag{16}$$

This provides us with a much more rigorous way of testing the proposed model, compared with that of a visual analysis, as we can compare the values from the model with those calculated for

[13]This can be verified easily using the right hand rule. If the thumb of the right hand is pointed in the direction of current flow along a long straight wire then the curl of the fingers represents the direction of the magnetic field.

[14]The magnetic field around a closed loop is proportional to the current which passes through the loop, as we move to the centre of the bar, assuming a uniform distribution of current, then we will have less current flowing through our loop, thus giving a lower field strength.

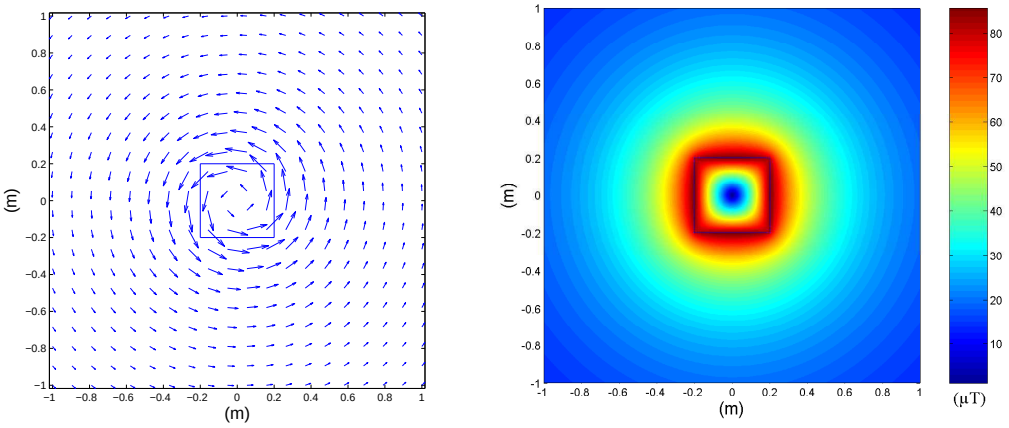

Figure 12: Magnetic field created by a $40cm$ by $40cm$ bar carrying $100A$, indicated by the blue square. Left: quiver plot of field, length of arrows proportional to field strength. Right: colour contour plot of magnetic field strength (in μT).

an infinite straight filament. If we subtract one from the other then close to the bar we should see a difference in the field caused by the different geometries of the bar and the wire. However, as we move away from the bar/wire then the difference should tend towards zero.

Figure 13 shows a comparison between the field model for a rectangular conductor of finite size (equations (13) & (14)) and the model of a filamentary conductor (equations (15) & (16)). At the top left we see the field model for a $0.1m$ x $0.1m$ bar carrying $30,000Amps$, and at the top right is the field model for a filamentary conductor also carrying $30,000Amps$. From a purely visual standpoint it is obvious that the two fields are very similar, which is what we would expect when looking at points far from the conductors (here the figures show the field up to $5m$ away on either side). The two bottom figures, however, show the difference between the calculated values for each of the two models, giving a more quantitative analysis. Once again the calculated values correspond very well with our predictions, close to the wire/bar the two models give different values due to the different geometries, but further away the difference tends towards zero (this is more evident in the figure at the bottom right). So upon first inspection it would appear that the model proposed here for the magnetic field created by a rectangular current carrying bar is correct for points far from the bar.

Having verified that our model is correct for points which are far away from the bar, it is now necessary to check that the model also gives the appropriate field for points close to the bar. In order to do this we shall compare the field calculated from equations (13) & (14) with that of a rectangular array of filamentary wires of the same dimensions as the bar and with the same total current (the current is divided equally between each of the filaments, again giving a uniform current distribution).

In figure 14 we see the difference between the magnetic field strength for a bar of $0.2m$ *by* $0.2m$ carrying $30,000amps$ calculated using our model, and that of an array of 400 (20 *by* 20) wires arranged to represent a bar of equal size and each carrying $75Amps$ giving a total of $400 \times 75 = 30,000Amps$. What we see is very much what we would have expected, outside of

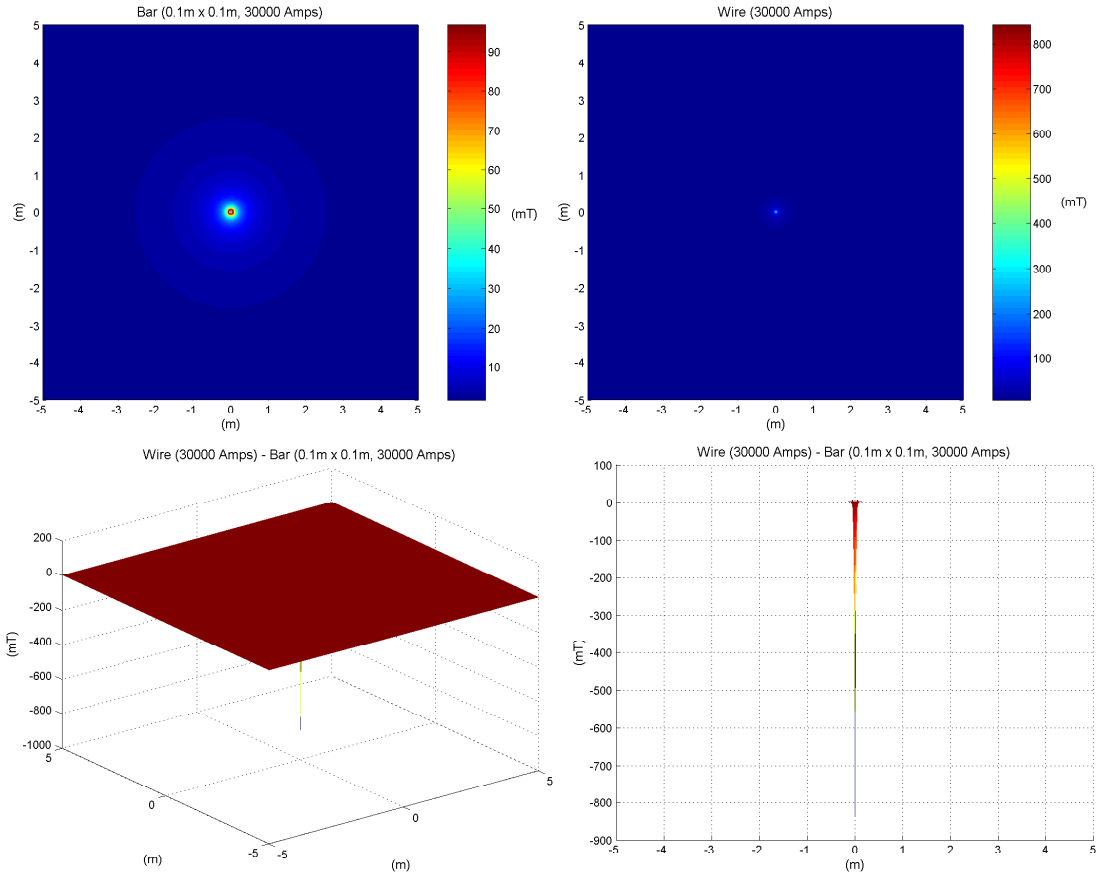

Figure 13: Comparison of the magnetic field calculated for a rectangular bar of finite size, and a filamentary wire. Top left: field (in mT) calculated for a $0.1m$ x $0.1m$ bar carrying $30,000 Amps$. Top right: field for a filamentary wire carrying $30,000 Amps$. Bottom left & right, graphic representation of the difference between the two calculated fields, from different perspectives.

the array of wires, the difference between the field strengths is zero. In order to understand why this is so, it is useful to make an analogy with the electric field of a uniformly charged sphere. If we take a uniformly charged sphere then the $\vec{E}$ field we see outside of the sphere is indistinguishable from the $\vec{E}$ field we would see from a point charge with the same total charge placed at the centre of the sphere. In our case, the wire array approximates a uniform distribution of current and so the field outside is indistinguishable. The field inside, however, is a different matter, we see the effects of the uneven charge distribution and thus we see a difference between the two field strengths.

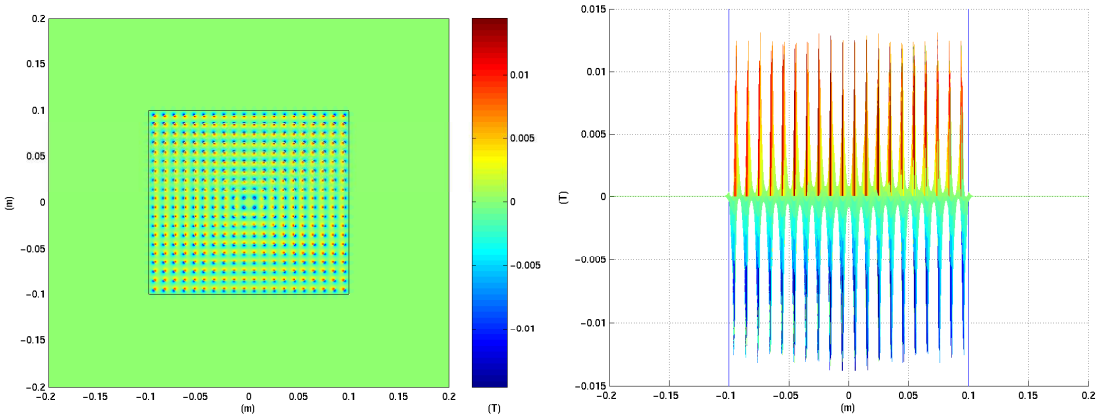

Figure 14: Left: Pseudo color plot of the difference between the field strength calculated using equations (13) & (14) for a bar of $0.2mx0.2m$ cross section carrying $30,000Amps$, and that of a rectangular array of the same dimensions, made up of 400 filamentary wires each carrying $75Amps$, the black square represents the position of the bar. Right: The same difference but from a side view, here the blue lines represent the edges of the bar.

Figure 15 shows the same plots as seen in figure 14, for a bar of the same dimensions and carrying the same current, but this time the wire array is made up of $100 \times 100 = 10,000$ wires. What we see is that the difference in the field strengths outside of the bars is again zero, for the same reasons mentioned above, but the difference in the field strengths inside the bar is this time much smaller (the right hand figures from both Fig. 14 and 15 are to the same scale). This is because we have a lot more wires and thus have a much better approximation of a uniform distribution of current. In fact, equation (10) is the limiting case of making the wires closer and closer together until we can perform an integral instead of a summation.

2.3 Extending the Computer Model to a System of Multiple Current Carrying Bars

Now that we have arrived at a suitable model for the field created by a single rectangular current carrying bar, it is a fairly simple process to extend this to find a model for the magnetic field from four current carrying bars. Since magnetic fields are linear in nature, it is sufficient to simply

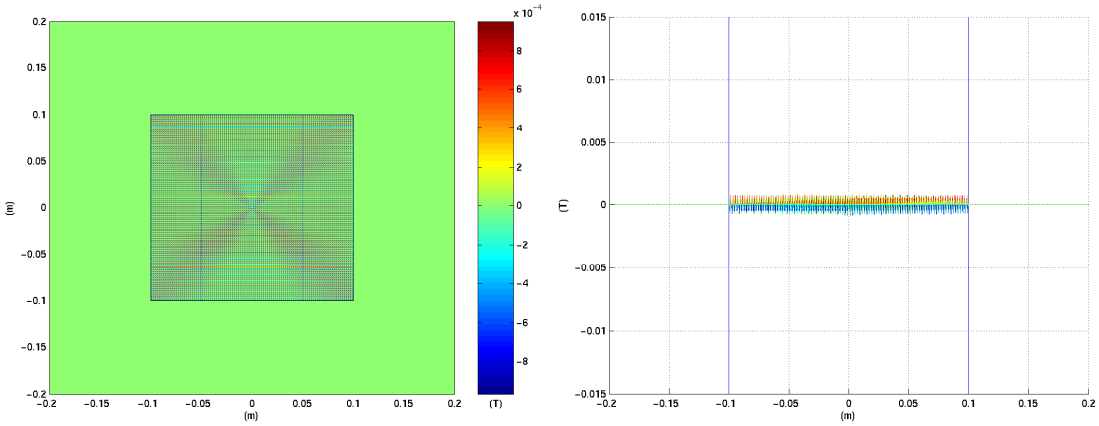

Figure 15: Left: Pseudo color plot of the difference between the field strength calculated using equations (13) & (14) for a bar of $0.2mx0.2m$ cross section carrying $30,000Amps$, and that of a rectangular array of the same dimensions, made up of 10,000 filamentary wires each carrying $3Amps$, the black square represents the position of the bar. Right: The same difference but from a side view, here the blue lines represent the edges of the bar.

add together the four separate fields for each of the four bars.[15] Using the real dimensions of the bars, and giving Bar 1 & Bar 2 a current of $30,000Amps$ and Bar 3 & Bar 4 a current of $-30,000Amps$, we finally arrive at a suitable model for the magnetic field created by this arrangement of four current carrying bars, a graphic representation of this model can be found in figure 16.

The model has shown to be robust when compared to the simpler cases of a single wire to test the field far from the bar, and an array of wires to test the field close to the bar. I am therefore confident that the magnetic field model proposed here is perfectly suitable for use in this project.

[15] Although the problem we are attempting to solve is caused by the the current of each bar being affected by the magnetic field of the others, in modeling the magnetic field it is not necessary, in our case, to take into account time dependance, and so we shall only look at the time independent situation.

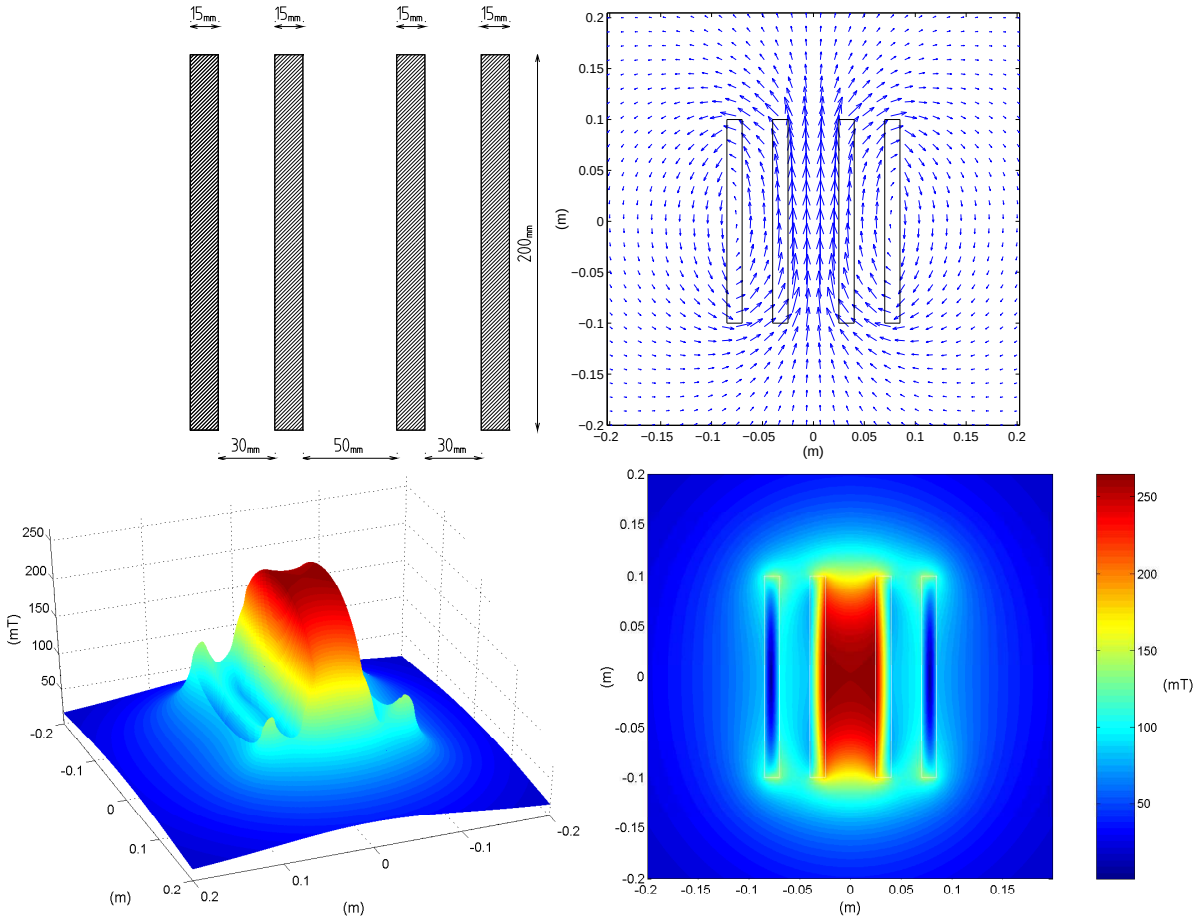

Figure 16: Magnetic field model for arrangement of four current carrying bars, each carrying $30,000 Amps$, the two bars on the left have current travelling out of the page, and the two on the right carry current into the page. Top left: Geometry of bars. Top right: Quiver plot of the magnetic field. Bottom left and right: magnetic field strength in mT.

3 Modeling the Probe Coils

Now that we have a suitable model of the magnetic field created by the current carrying bars, the next step is to create a model for the probe coils, so that we can find an appropriate arrangement of probe coils to satisfy the problem.

The probe coils are made up of loops of wire and work on the principle of magnetic induction, whereby:

> The induced emf ε in a closed loop of wire equals the negative of the rate of change of the magnetic flux Φ passing through the loop (Faraday's induction law).

The magnetic flux is defined as follows in equation (17).

$$\Phi = \int B_{\perp} dA = \int B \cos\phi dA = \int \vec{B} \cdot d\vec{A} \tag{17}$$

Faraday's induction law is then given by equation (18).

$$\varepsilon = -\frac{d\Phi}{dt} \tag{18}$$

By adding an integration circuit to the loop we can then use the measured voltage as an indirect measure of the magnetic field at the position of the loop.

3.1 A Simple Probe Coil Model

In order to model the probe coils it is adequate to simply calculate the magnetic flux which would pass through them. This is a fairly simple operation, as we already have a model of the magnetic field, and the flux is simply the surface integral of the magnetic field perpendicular to the surface bounded by the loop. In our case we can assume by geometry that all of the loops will be perpendicular to the y component of the $\vec{B}$ field, and so we can disregard the x component, as this will not be seen by the loop.

Using our magnetic field model in MATLAB, we can essentially carry out a numerical integration of the field over the surface of the loop. We do this by calculating the field B_y at a series of points inside the surface bounded by the loop, multiplying each value by the area that value represents δA(essentially calculating the flux through each very small area), and then adding together all of the contributions in order to calculate the total flux. We can make a simplification in our case, since the field does not vary along the $z - axis$, we can simply calculate the flux in the $x - y$ plane and then multiply by the length, Z, of the loop along the $z - axis$ (making the area of each small contribution $Z\delta l$ where δl is a small width of the loop along the $x - axis$). This can be more clearly seen in figure 17. We therefore arrive at the following equation (19) for the flux through each loop:

$$\Phi_{rect} = \sum_{i=1}^{n} B_{y_i} Z\delta l = Z\delta l \sum_{i=1}^{n} B_{y_i} = \frac{Zl}{n} \sum_{i=1}^{n} B_{y_i} \tag{19}$$

This can be easily extended to more than one loop (a coil), since a coil can be treated as a series of loops and the total emf will be equal to the sum of all the separate emfs.

$$\varepsilon = \sum_{j=1}^{k} \varepsilon_j = -\sum_{j=1}^{k} \frac{d\Phi_j}{dt} = -\frac{d}{dt}\sum_{j=1}^{k} \Phi_j = -\frac{d\Phi_{recttotal}}{dt} \tag{20}$$

We can therefore simply add together the flux through each loop and look at the total flux. If we take n to be the number of calculated values of the magnetic field within each loop, and k to be the number of loops, then the total flux will be:

$$\Phi_{recttotal} = \sum_{j=1}^{k} \Phi_j = \sum_{j=1}^{k} \left(\frac{Zl}{n} \sum_{i=1}^{n} B_{y_i} \right)_j = \frac{Zl}{n} \sum_{i=1,j=1}^{n,k} B_{y_{i,j}} \tag{21}$$

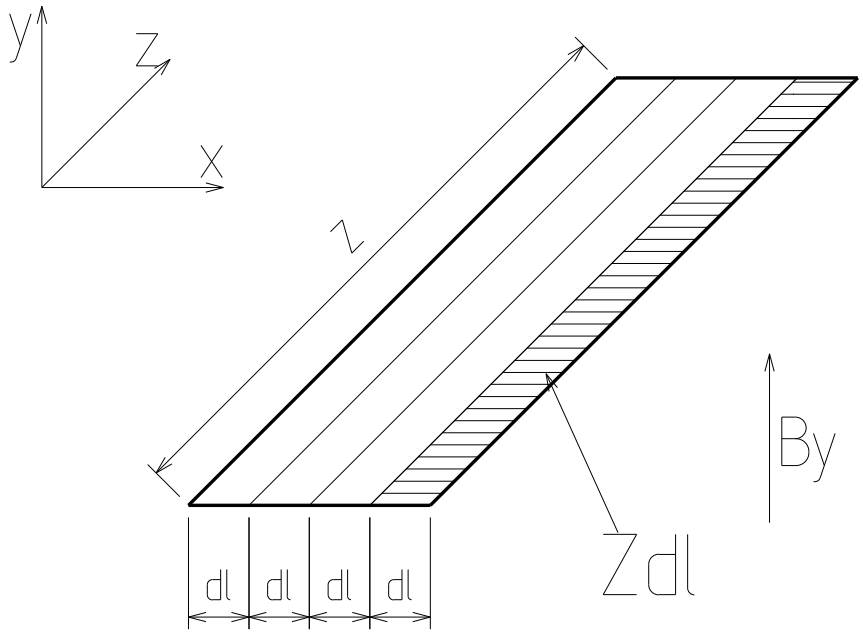

Figure 17: The bold line represents the position of the coil, here we can clearly see the values Z and δl as well as the area $Z\delta l$.

Thus, via a simple manipulation of the magnetic field model we have already created within MATLAB, we can model a simple probe coil made up of rectangular loops. We can once again carry out a quick check of the validity of this model by comparing the values calculated for our model to those calculated in a simpler case. If we take a single loop of area $1m^2$ at $50m$ (coordinates of the centre of the loop being $(50, 0, 0)$) from a wire carrying $1,000,000Amps$, and placed such that the area bounded by the coil is perpendicular to the y component of the magnetic field, the coil sees a B_y component of the field given by[16]:

[16]In this paper, it is assumed that the surface vector of the loop points in the positive y direction, that is to say that a B_y component pointing in the positive y direction will produce a positive flux

$$B_y = \frac{\mu I}{2\pi}\frac{x}{x^2+y^2} = -\frac{4\pi \times 10^{-7} \times 10^6}{2\pi}\frac{50}{50^2+0^2} = \frac{2 \times 10^{-1}}{50} = 0.004T$$

The flux will then be:

$$\Phi = \int \vec{B} \cdot d\vec{A} = B_y A = 0.004T \times 1m^2 = 0.004Wb$$

For the MATLAB calculation, the exact same conditions were used, with a value of $n = 500$ and $k = 1$, and the model reached the same value of $0.004Wb$ [17]. So it would appear that the proposed model for the probe coil is robust. The model can be easily expanded to more than one coil, by essentially carrying out the calculation for each coil and then adding all of the coils together.

3.2 A More Realistic Probe Coil Model

The next step is to apply the simple model above to the real world situation. For a start, the probe coils currently in place do not have a rectangular loop area, instead the loop is in the shape of a rectangle with a trapezium at each end (see figure 18). This was done to reduce the curvature of the wire used so that the wire could be wound tighter and stay closer to the original area. Assuming that the current probe coils were constructed in the way that they were due to reasons of practicality, it is logical to design the new coils in the same way. We must also take into account the diameter of the wires, the new probe coils will be constructed from $0.3mm$ wire, but the packing diameter is $0.339mm$[18], this is because $0.3mm$ is the internal diameter of the wire, not taking into account the insulation, and also because the wires will not pack together exactly.

Figure 18: General shape of the probe coils.

It is a relatively simple step to extend our rectangular model to incorporate the trapezium sections at each end. Let us first look at the single loop case, to simplify matters we may look at the rectangular section and the two trapezia as being separate parts and treat the rectangular section in the same way as above. In order to calculate the flux passing through the trapezium section we can create a matrix of points at which we will calculate the magnetic field, we can then overlay the shape of the trapezium onto this matrix and only take into account the points

[17] Actual value calculated was 0.00400013334080 Wb, but this can be attributed to the variation in the magnetic field strength over the area of the loop

[18] This diameter was calculated by measuring the diameter of a coil of 75 loops of 0.3mm wire, which had a total width of 25.45mm

which fall inside the boundaries. In the same way as with the rectangular section we must then multiply each of the points by the area that point represents. If we make the assumption that each point represents the same area[19], then each point will represent an area of:

$$\delta A_T = h_T \frac{a_T + b_T}{2n_T} \tag{22}$$

Where h_T is the height of the trapezium along the $z - axis$, a_T & b_T are the width of the top and the bottom of the trapezium, and n_T is the number of points of the matrix which lie within the trapezium. Thus the flux passing through each trapezium shaped section of the coil will be:

$$\Phi_{trap} = \delta A_T \sum_{l=1}^{n_T} B_{y_l} \tag{23}$$

If we make the assumption that the trapezia at either end of the coil are identical, then due to the symmetry of the problem, each of the trapezia will see exactly the same flux, and so we can simply multiply the flux from one trapezium by two to get the total flux through the two trapezia. Therefore the total flux passing through the $2k$ trapezia (where k is the total number of loops in the probe coil) is given by (24):

$$\Phi_{traptotal} = 2\delta A_T \sum_{l=1,j=1}^{n_T,k} B_{y_{l,j}} \tag{24}$$

Combining the flux from the trapezium and rectangular sections, we arrive at the following expression (equation (25)) for the total flux passing through a probe, with a cross section as shown in figure 18, and with k loops in total:

$$\Phi_{total} = \sum_{j=1}^{k} \left(\frac{Zl}{n} \sum_{i=1}^{n} B_{y_{i,j}} + 2\delta A_T \sum_{l=1}^{n_T} B_{y_{l,j}} \right) \tag{25}$$

To turn this equation into a model in MATLAB, we need to determine at which points to calculate B_y. This is not an entirely trivial matter as the model must be representative of the real world situation, and thus many factors need to be taken into account. Let us first look at the positions for $B_y(x_i, y_j)$ which represent the values of B_y calculated within the rectangular sections of the probe coils. In this case each x_i represents a position along the $x - axis$ and each value of y_j will represent the position of a coil along the $y - axis$ (see figure 17 for clarification on the axis system used in this model). Let us start with the positions along the $x - axis$, each one must represent the same area, $z\delta l$, within the rectangular loop. In order for each point to represent the same area the points must be placed in the middle of each of the small rectangular areas $z\delta l$. If the coordinate of the left hand edge of the loop is $x1$ and the coordinate of the right hand edge of the loop is $x2$ then each section of the $x - axis$, δl, will have a length of:

$$\delta l = \frac{x2 - x1}{n} \tag{26}$$

[19]This may not be exactly the case for points next to the boundary of the trapezium, but the effect this approximation has should be negligible and so we will neglect this effect

The center of the first small rectangle on the left is $x1 + \frac{\delta l}{2}$, the center of the small rectangle directly adjacent to the right is $x1 + \frac{\delta}{2} + \delta l = x1 + \frac{\delta l + 2\delta l}{2}$, and the position along the $x - axis$ of the center of the ith rectangle is:

$$x_i = x1 + \frac{\delta l + 2(i-1)\delta l}{2} \tag{27}$$

For the k positions of the coils along the $y - axis$ let us take $y1$ to be the position of the bottom of the probe coil, and $y2$ to be the position of the top of the probe coil.[20] Taking a packing width of 0.00034m the number of coils, k, can be calculated as[21]:

$$k = \frac{y2 - y1}{0.00034} \tag{28}$$

We wish to calculate the magnetic field at the position of the center of the wire which makes up each of the loops, the appropriate k positions along the $y - axis$ can then be calculated in a similar way to the i positions along the $x - axis$. We shall use the matrix convention for indices, and so $j = 1$ will refer to the position of the top loop in the probe coil, and $j = k$ will refer to the bottom loop in the probe coil. Using this convention, the position of loop $j = 1$ should be $y2 - \frac{\delta y}{2}$ where $\delta y = 0.00034m$ is the packing width of the wire. The position of loop $j = k$ will therefore be $y1 + \frac{\delta y}{2}$, but since $y1 = y2 - \delta yk$ we can rewrite the position of loop $j = k$ as $y2 - \delta yk + \frac{\delta y}{2} = y2 - \frac{\delta y(2k-1)}{2}$. The jth coil will then have a position along the $y - axis$ of:

$$y_j = y2 - \frac{\delta y(2j-1)}{2} \tag{29}$$

x_i and y_j give the positions at which we need to calculate the magnetic field for the rectangular sections, the symmetry of the rectangular sections implies that we can neglect the $z - axis$, this is not the case, however, when we look at the trapezoidal sections. We can use the same positions y_j for the loops in the trapezium sections, however we must now look at points along both the x & z axis. In order to treat the trapezium shaped parts of the coils, we shall create a matrix of positions in the $x - z$ plane, at which we wish to calculate the magnetic field. The shape of the trapezium shall then be effectively overlayed onto this matrix of points, and only points which fall inside the trapezium shall be taken into account. Let us look at an example case, in which we shall take the number of loops in the coil $k = 10$, the number of points in our matrix along the $x - axis$ shall be $n = 10$ and the number of points along the $z - axis$ will be $r = 10$. If $h_T = 0.005m$, $a_T = 0.01m$, and $b_T = 0.005m$ then we arrive at the following $r \times n$ matrix $\mathbf{M}$, representing, in the $x - z$ plane, the points which fall within the trapezium with a 1 and the points outside the trapezium with a 0.

[20] We define the position of the top of the probe coil to be the top surface of the top loop within the probe coil, and similarly for the bottom of the coil.

[21] The model of the probe coil created in MATLAB actually works in the opposite sense, using the number of coils k to calculate the values of $y2$ & $y1$.

$$\mathbf{M} = \begin{pmatrix} 1 & 1 & 1 & 1 & 1 & 1 & 1 & 1 & 1 & 1 \\ 1 & 1 & 1 & 1 & 1 & 1 & 1 & 1 & 1 & 1 \\ 0 & 1 & 1 & 1 & 1 & 1 & 1 & 1 & 1 & 0 \\ 0 & 1 & 1 & 1 & 1 & 1 & 1 & 1 & 1 & 0 \\ 0 & 1 & 1 & 1 & 1 & 1 & 1 & 1 & 1 & 0 \\ 0 & 1 & 1 & 1 & 1 & 1 & 1 & 1 & 1 & 0 \\ 0 & 0 & 1 & 1 & 1 & 1 & 1 & 1 & 0 & 0 \\ 0 & 0 & 1 & 1 & 1 & 1 & 1 & 1 & 0 & 0 \\ 0 & 0 & 1 & 1 & 1 & 1 & 1 & 1 & 0 & 0 \\ 0 & 0 & 1 & 1 & 1 & 1 & 1 & 1 & 0 & 0 \end{pmatrix}$$

Now assuming that the same value of n has been used for both the rectangular and the trapezium sections, we will have already calculated all the values of the magnetic field that we need. We can essentially treat each row along the $z - axis$ as a slice of the magnetic field in the $x - y$ plane, which we have already calculated. So for each slice we simply keep the values which fall inside the trapezium, and disregard those that don't. For example for the row $m = r = 10$ we have the following:

$$\begin{pmatrix} 0 & 0 & 1 & 1 & 1 & 1 & 1 & 1 & 0 & 0 \end{pmatrix}$$

If we replicate this row k times to create a $k \times n$ matrix, representing the $x - y$ plane, we arrive at the following matrix:

$$\mathbf{M_{10}} = \begin{pmatrix} 0 & 0 & 1 & 1 & 1 & 1 & 1 & 1 & 0 & 0 \\ 0 & 0 & 1 & 1 & 1 & 1 & 1 & 1 & 0 & 0 \\ 0 & 0 & 1 & 1 & 1 & 1 & 1 & 1 & 0 & 0 \\ 0 & 0 & 1 & 1 & 1 & 1 & 1 & 1 & 0 & 0 \\ 0 & 0 & 1 & 1 & 1 & 1 & 1 & 1 & 0 & 0 \\ 0 & 0 & 1 & 1 & 1 & 1 & 1 & 1 & 0 & 0 \\ 0 & 0 & 1 & 1 & 1 & 1 & 1 & 1 & 0 & 0 \\ 0 & 0 & 1 & 1 & 1 & 1 & 1 & 1 & 0 & 0 \\ 0 & 0 & 1 & 1 & 1 & 1 & 1 & 1 & 0 & 0 \\ 0 & 0 & 1 & 1 & 1 & 1 & 1 & 1 & 0 & 0 \end{pmatrix}$$

We can then take the element by element product between the matrix $\mathbf{M_{10}}$ and the matrix $\mathbf{B_{xy}}$ to get $\mathbf{B_{10}} = \mathbf{M_{10}} \cdot \mathbf{B_{xy}}$, where $\mathbf{B_{xy}}$ is the matrix containing the magnetic field calculated at the points within the $x - y$ plane. The matrix $\mathbf{B_{10}}$ therefore represents the magnetic field at the points which fall within the 10th slice, with a zero at the points outside the trapezium in this plane, and the value of the magnetic field at the points within the trapezium in this plane. To put all of this into the summation notation used previously, we shall define the following:

- $\mathbf{M_m}$ is the $k \times n$ matrix made up of row m of the matrix $\mathbf{M}$ replicated k times.
- $\mathbf{B_m}$ is the dot product $\mathbf{M_m} \cdot \mathbf{B_{xy}}$ where $\mathbf{B_{xy}}$ is the $k \times n$ matrix containing the values of the y component of the magnetic field $B_y(x_i, y_j)$.

If we incorporate all of the reasoning above, the expression for the total flux, in a form which can be incorporated into a MATLAB model, is as follows:

$$\Phi_{total} = \frac{Zl}{n} \sum_{j=1,i=1}^{k,n} B_y(x_i, y_j) + 2\delta A_T \sum_{m,i,j}^{r,n,k} \mathbf{B_m}(i,j) \tag{30}$$

Where:

- $B_y(x_i, y_j)$ is the value of the y component of the magnetic field calculated at the position (x_i, y_j).
- n_T can be found by summing the contents of the matrix $\mathbf{M}$.
- $\mathbf{B_m}(i,j)$ refers to the component of the matrix $\mathbf{B_m}$ at the position (i,j), using matrix index notation.

The expression above can be incorporated into a MATLAB model, allowing us to model a realistic magnetic probe within our model of the magnetic field created by 4 current carrying bars. The next step is to test the model, to see what kind of results we get and whether they correspond with our expectations.

Since we have already thoroughly tested the model for the magnetic field of the current carrying bars it is only necessary to test whether the probe coil model appropriately sums the flux contributions. We can make this assumption as the only new thing introduced into the model of the probe coils is at which points we need to calculate the magnetic field, therefore it is sufficient to simply test whether the probe coil model gives the expected flux in the case of a constant, uniform magnetic field. In the case of a constant magnetic field, perpendicular to the probe coil, the model should return a value equal to the magnetic field strength multiplied by the total surface area. Table 1. gives calculated and expected values for various configurations of the probe coil model:

No. of coils (k)	Area per coil (m^2)	Total area (m^2)	B_y (T)	Expected Flux (Wb)	Calculated Flux (Wb)
1	0.115	0.115	1	0.115	0.115
5	0.115	0.575	1	0.575	0.575
20	0.26	5.2	3	15.6	15.6
50	0.26	13	-3	-39	-39

Table 1: Calculated and expected values for the flux, in the case of a constant, uniform magnetic field.

The table clearly shows that the model appropriately represents the geometry of the situation, and as such confirms the model to be appropriate for the work carried out here. If we take a

look at the first two configurations, we can see that 5 coils gives 5 times the flux of one coil, exactly as expected, and in the final configuration we see that the model appropriately takes into account the direction of the $\vec{B}$ field, by giving a negative flux value for a magnetic field in the negative y direction.[22].

3.3 Mutual Inductance

We shall now look at how the system reacts to magnetic fields created by different distributions of current. It is interesting at this point to introduce the concept of mutual inductance which gives us a relationship between the current flowing in a bar and the flux that will be seen by a probe coil. The mutual inductance M between the probe coil and the current carrying bar can be written as follows:

$$M = \frac{\Phi_{total}}{I} \tag{31}$$

Where I is the current flowing in the bar. Using the model as developed so far it is a fairly easy exercise to calculate the mutual inductance, we simply calculate the flux seen by the probe coil for a given current and then use equation (31) to find the mutual inductance. This can be further extended to a system of multiple current carrying bars, in order to work out the mutual inductance between the probe coil and each of the bars we simply set the current in all but one of the bars to zero, then divide the flux in the probe by the current flowing in the bar for which we wish to calculate the mutual inductance. At this point I shall introduce a system of notation for the mutual inductances M_{A1}, where the letter represents the probe coil and the number represents the current carrying bar. Knowing the mutual inductances allows us to work out what distribution of currents would give rise to a certain flux. If we had one probe coil and four current carrying bars, then the total flux would be given by:

$$\Phi_{total} = M_{A1}I_1 + M_{A2}I_2 + M_{A3}I_3 + M_{A4}I_4$$

Well now that we have spoken a little about the concept of mutual inductance, lets take a look at how it works in our model. Let us work out the mutual inductances between a probe coil and each of the four current carrying bars in the system we would like to analyze. Figure 19 shows the arrangement of four current carrying bars, along with the test coil, which is made up of 500 turns (the exact dimensions of the probe coil are of no interest at this point).

Using the method mentioned above, we find that the mutual inductances for this probe coil are:

M_{A1} (H)	M_{A2} (H)	M_{A3} (H)	$M_{A4}(H)$
-1.0390×10^{-5}	-0.7300×10^{-5}	-0.4950×10^{-5}	-0.3994×10^{-5}

Table 2: The mutual inductances of a single probe coil arranged next to four current carrying bars.

What we see from the calculated mutual inductances is fairly logical, the mutual inductance between the probe coil and the bar closest to it is the greatest, and vice-versa for the bar furthest

[22]In this model, the direction of positive flux is defined to be in the direction of the positive $y - axis$.

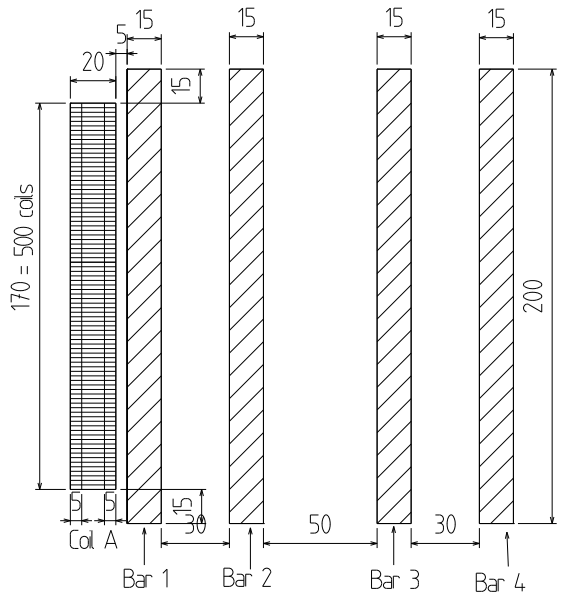

Figure 19: Arrangement of four current carrying bars, along with probe coil A. All measurements in mm.

away. So on first inspection we seem to be on the right track, the next step is to test the system for different distributions of current between the four bars and see if the flux calculated directly from the model corresponds with the flux calculated from the mutual inductances. Table 3.3 shows just this:

I_1 (A)	I_2 (A)	I_3 (A)	I_4 (A)	Flux calculated from mutual inductances (Wb)	Flux calculated from probe coil model (Wb)
$30,000$	$30,000$	$-30,000$	$-30,000$	-0.262418	-0.262418
$30,000$	0	$30,000$	0	-0.460187	-0.460187
100	200	300	400	-5.58126×10^{-3}	-5.58126×10^{-3}
$60,000$	0	0	$30,000$	-0.743221	-0.743221

Table 3: Comparison of the flux calculated using the probe coil model with the flux calculated using the mutual inductances.

What we see in table in table 3.3 is that our system for calculating and manipulating the mutual inductances between a probe coil and each of the current carrying bars appears to work correctly. In this section we have created a robust model of a probe coil, which correctly calculates the magnetic flux which would pass through it. Although this model has been tested for the case of a set of current carrying bars, such as those in the system we would like to measure, it is independent of the magnetic field model used. The next step is to use this probe coil model, along with the magnetic field model developed in the previous section, to find a suitable set of probe coils to fulfil the conditions set out in our original problem.

4 Modeling a Complete System of Probe Coils

4.1 Modeling the Currently Installed System

Having successfully created a model of the magnetic field and the probe coils, we can now create a model of a system of multiple probe coils arranged around the current carrying bars. Let us start with a model of the system currently in place, this will give us an idea as to why the current system doesn't work and thus of how to make a system which does. Figure 20 shows the dimensions[23] of the current probe coils, each coil is made up of 500 loops of wire wound onto a plastic core.

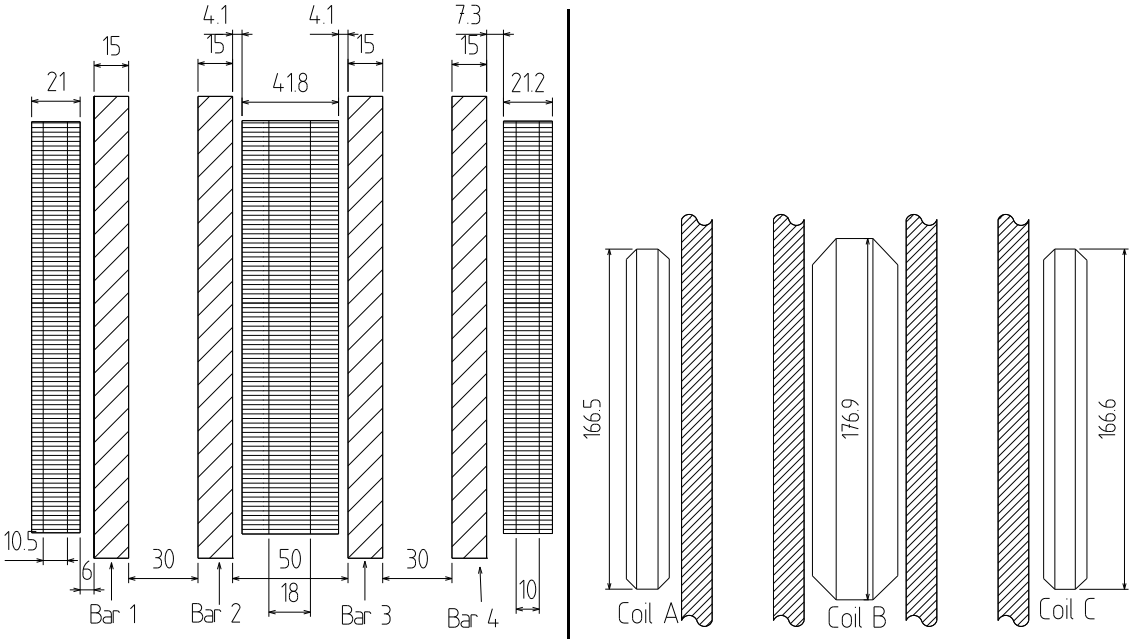

Figure 20: Current system of probe coils. Left: Front on view of the coils, from left to right: coil A, coil B, coil C, each coil is made up of 500 loops. Right: Top view of probe coils. All measurements in mm.

The probe coils are connected together such that the the surface vectors of the loops in coils A and C are opposite to the surface vectors of the loops in coil C. This is done to remove any effect which would be caused by the flux from an external magnetic field, as in this configuration the total surface is almost null. The total surface area of coil A is $1.7216m^2$, the area of coil B is $3.5505m^2$, and the area of coil C is $1.7364m^2$. If we add together the areas of coil A and C, then subtract the area of coil B then we get the total surface area of the system of probe coils as $0.0925m^2$. The total surface area is an important consideration in our system, as the probe coils are near to the large magnetic fields used by the Tokamak to contain the plasma, and we do not wish to pick up flux from these fields, so a null or near null total surface area will remove this problem.

[23]The dimensions given are actually those of the plastic core, onto which the loops of wire are wound.

We shall adopt the convention that the surface vectors of the loops in coils A and C point in the positive y direction, and that the surface vectors of the loops in coil B point in the negative y direction. The mutual inductances however shall be calculated assuming that all surface vectors point in the positive y direction. This aids with notation, as in the equation of the total flux the contributions from probe coils pointing in the negative y direction will be negative (this can be seen in equation (32)). In this case the total flux can be written in terms of currents and mutual inductances as follows:

$$\begin{aligned}\Phi_{total} = \quad & M_{A1}I_1 + M_{A2}I_2 + M_{A3}I_3 + M_{A4}I_4 \\ & -M_{B1}I_1 - M_{B2}I_2 - M_{B3}I_3 - M_{B4}I_4 \\ & +M_{C1}I_1 + M_{C2}I_2 + M_{C3}I_3 + M_{C4}I_4\end{aligned} \tag{32}$$

Using the method described in the previous section, we find that the mutual inductances of the current system are:

M_{A1}:	-4.332×10^{-6}	M_{A1}:	-3.053×10^{-6}	M_{A1}:	-2.075×10^{-6}	M_{A1}:	-1.676×10^{-6}
M_{A1}:	5.961×10^{-6}	M_{A1}:	8.343×10^{-6}	M_{A1}:	-8.344×10^{-6}	M_{A1}:	-5.961×10^{-6}
M_{A1}:	1.680×10^{-6}	M_{A1}:	2.078×10^{-6}	M_{A1}:	3.050×10^{-6}	M_{A1}:	4.316×10^{-6}

Table 4: Mutual Inductances of the current system of probe coils (H)

We can see the problem with the current system if we look at table 5, the table shows the flux calculated for different distributions of current. The current supplied to the magnetic field coils is the sum of bars 1 & 2, or the negative of the sum of bars 3 & 4, therefore we want a system that gives the same flux measurement for different distributions of the same total current. What we see in table 5 is that the current system does not do this, this is because the current system was designed on the assumption that the current would be equally distributed within the two pairs of bars. This is not the case when the current changes rapidly during the ramping up or down of the power supply. During this time the rapidly changing current induces a magnetic field which alters the distribution of current between the bars. Therefore, instead of measuring two currents with 3 probe coils, we are actually measuring 4 currents with 3 probe coils, which it would seem does not work.

What we need is to find an arrangement of coils such that the flux is dependent on the currents $I_{left} = I_1 + I_2$ and $I_{right} = I_3 + I_4$, and not the individual currents. We can make a few assumptions in our case. Due to symmetry we can assume that: $I_1 = -I_4$, $I_2 = -I_3$, and due to conservation of charge: $I_{left} = -I_{right}$. If we look at figure 21 we can see that the flux appears to depend linearly upon the current distribution, the figure shows the flux plotted against I_1,

I_1 (Amps)	I_2 (Amps)	I_3 (Amps)	I_4 (Amps)	Flux (Wb)
0	60,000	-60,000	0	-1.1182
30,000	30,000	-30,000	-30,000	-1.0755
60,000	0	0	-60,000	-1.0328

Table 5: Total flux in current system of probe coils, calculated for different distributions of the same total current: bar 1 + bar 2 = 60,0000 Amps, bar 3 + bar 4 = -60,000 Amps.

with $I_{left} = -I_{right} = 60,000 Amps$. What we want is for this plot to be flat, so that the flux does not depend on any of the individual currents, and only on the currents I_{left} and I_{right}. For this we need to add in a second system to balance the first, what we need is a supplementary arrangement of coils, which gives a gradient which is opposite to the gradient of the first system.

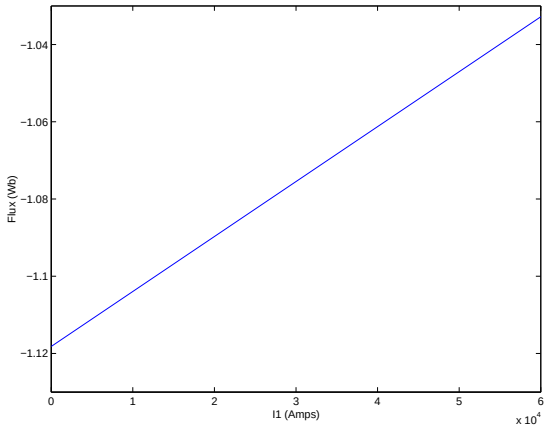

Figure 21: Plot of flux against I_1 for the current system of probe coils, with an $I_{left} = -I_{right} = 60,000 Amps$

4.2 Modeling a New System of Probe Coils

What we shall do is design two new systems of three probe coils each. The first system shall be based upon the current system of three probe coils, one in the middle of bars 2 & 3, and one at each side of the current carrying bars. The second system will also have three bars, with one in the middle of bars 2 & 3, one in the middle of bars 1 & 2, and the other in the middle of bars 3 & 4. We shall then tweak the dimensions of the two systems until we arrive at a complete system of probe coils for which the flux is independent of the current distribution. The total system must also have a total surface area equal to zero, for the reasons laid out previously. The system must also be constructible, so all dimensions will be calculated such that they are as close as possible to $5mm$ units.

4.2.1 System 1

Lets start with the first system, we have quite a lot of freedom when it comes to the dimensions of the first system, and so we shall try and design something which best fits the design criteria. As the two systems shall be designed separately, it is sufficient to ensure that the surface area of each system is zero. I have decided to fix the dimensions of the trapezium sections and the width of each of the probe coils, as can be seen in figure 22. I shall also give all of the probe coils in the system the same number of loops. The two coils on either side of the current carrying bars have been made identical, to make construction easier. Thus the only parameter which we shall vary is the length of the probe coil along the z-axis.

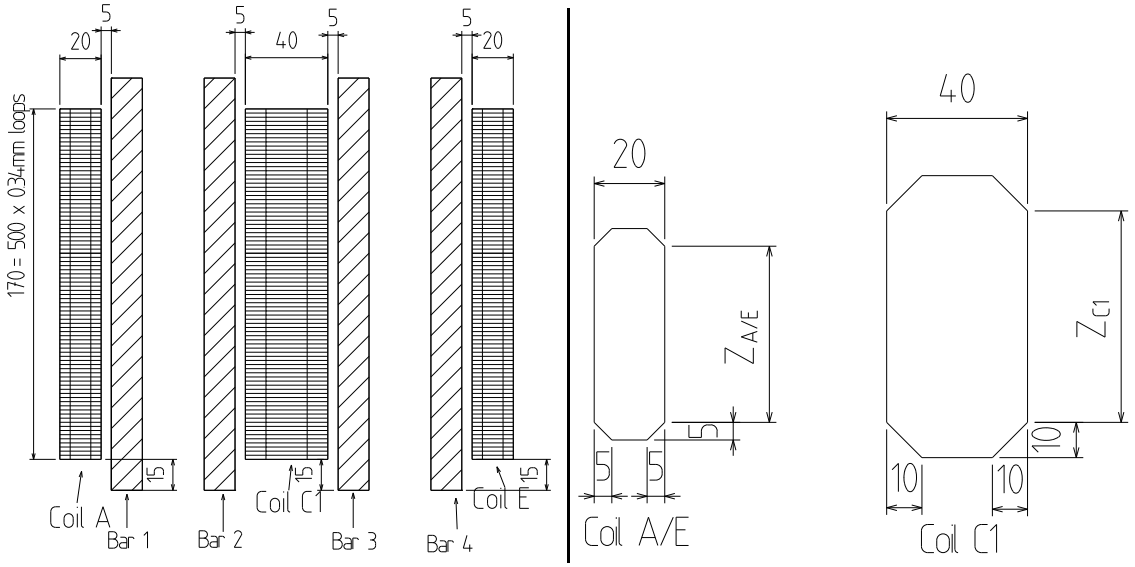

Figure 22: System 1. Left: Front view of the arrangement of probe coils for system 1, all coils made up of 500 loops. Right: Dimensions of the trapezia section for the three probe coils in system 1, the only variables shall be $Z_{A/E}$ and Z_{C1}. All dimensions in mm.

Figure 22 shows the arrangement of coils for system 1, in relation to the current carrying bars. It also shows the fixed dimensions for the trapezium sections of the probe coils. Only one diagram is shown for both coil A and coil E, as these two coils are identical. The naming of the coils is based on the fact that there will be more coils in between, and will become clearer as we move onto system 2. Although both $Z_{A/E}$ and Z_{C1} seem to be presented as variables, they are in fact dependent upon one another due to the constraint that the total area must be equal to zero. The total area is given by:

$$Area_{system1} = N_{coils_{AE}}(4Area_{trap_{AE}} + 2Area_{rect_{AE}}) - N_{coils_{C1}}(2Area_{trap_{C1}} + Area_{rect_{C1}})$$

Where:

- $N_{coils_{AE}} = N_{coils_{C1}} = 500$
- $Area_{trap_{AE}} = 5\frac{(10+20)}{2} = 75mm^2$
- $Area_{trap_{C1}} = 10\frac{(20+40)}{2} = 300mm^2$
- $Area_{rect_{AE}} = 20Z_{A/E}mm^2$
- $Area_{rect_{C1}} = 40Z_{C1}mm^2$

So for the total area to be 0:

$$4 \times 75 + 2 \times 20Z_{A/E} - 2 \times 300 - 40Z_{C1} = 0$$
$$40Z_{A/E} - 40Z_{C1} - 300 = 0$$
$$\boxed{Z_{C1} = Z_{A/E} - 7.5mm} \qquad (Z_{A/E} \ \& \ Z_{C1} \ in \ mm)$$

Thus for the constraints detailed previously, we have a relationship between the variables Z_{C1} and $Z_{A/E}$. This is useful as it allows us to define system 1 using only one variable. Let us take a look at what difference the alteration of $Z_{A/E}$ makes to the system. In figure 23 we see the flux of system 1 plotted against I_1, with $I_{left} = -I_{right} = 60,000 Amps$. In the plot on the left $Z_{A/E} = 0.2m$, and in the plot on the right $Z_{A/E} = 0.4m$, as expected the flux is greeter for the case where $Z_{A/E} = 0.4m$ as the total surface area is greater. What we are more interested in however is the fact that the gradient, $\Delta\Phi_1$ in the two cases is different, for $Z_{A/E} = 0.2m$ $\Delta\Phi = 1.449 \times 10^{-6}$ and for $Z_{A/E} = 0.4m$ $\Delta\Phi = 2.848 \times 10^{-6}$.

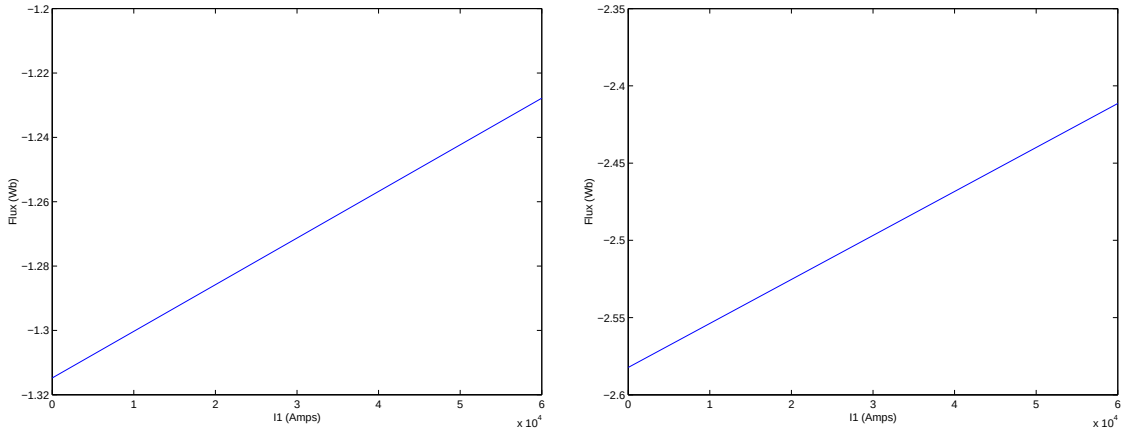

Figure 23: Left: Plot of total flux against I_1 with $I_{left} = -I_{right} = 60,000 Amps$ and $Z_{A/E} = 0.2m$. Right: Plot of total flux against I_1 with $I_{left} = -I_{right} = 60,000 Amps$ and $Z_{A/E} = 0.4m$.

In fact, if we plot $\Delta\Phi_1$ against $Z_{A/E}$, we find that there is a linear relationship between the two values (see figure 24). This will come in very useful when finding an appropriate system 2, as the necessary requirement for the flux to be independent of the current distribution is that $\Delta\Phi_1 = -\Delta\Phi_2$, where $\Delta\Phi_2$ is the gradient of the equivalent plot for system 2. Using the data from figure 24 we find that the relationship between $\Delta\Phi_1$ and $Z_{A/E}$ is:

$$\Delta\Phi_1 = 6.995 \times 10^{-6} Z_{A/E} + 5.02 \times 10^{-8} \qquad (Z_{A/E} \ \ in \ \ m) \tag{33}$$

4.2.2 System 2

Let us now look at system 2, this system will once again be made up of three probe coils, and as in the previous case all dimensions will be fixed except for the lengths Z_{BD} and Z_{C2}, which we will see are linked in a similar way to Z_{AE} and Z_{C1}. Figure 26 shows us the layout of the coils for system 2. The first noticeable difference between system 1 and system 2 is that the probe coils are not all made up of the same number of loops. This is because probe coil C2 will not form part of the final system in itself, instead it shall be incorporated with probe coil C1 to produce probe coil C. Since the trapezoidal sections of coil C will be identical to those of coil C1, incorporating C2 is equivalent to changing the length Z_C, in other words adding or subtracting a rectangular section. Thus coil C2 has a rectangular cross section and is made up

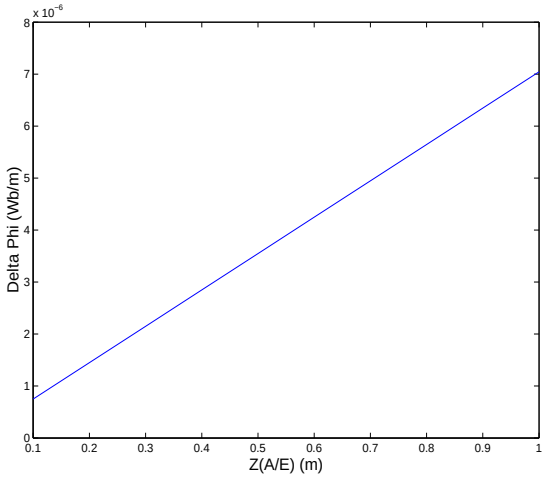

Figure 24: $\Delta\Phi_1$ plotted against $Z_{A/E}$ for system 1.

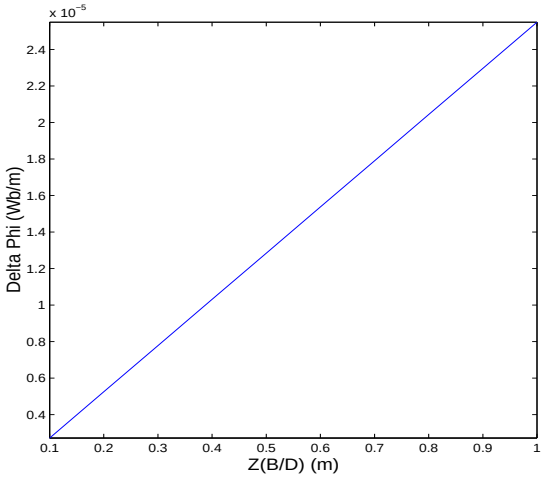

Figure 25: $\Delta\Phi_2$ plotted against $Z_{B/D}$ for system 2.

of the same number of loops as coil C1. Other than this we shall proceed with the analysis of system 2 in the same way as we did with system 1.

The first step is to find a relationship between Z_{BD} and Z_{C2}, let us start in the same way as we did for system 1. The total surface are of system 2 is given by:

$$Area_{system2} = N_{coils_{BD}}(4Area_{trap_{BD}} + 2Area_{rect_{BD}}) - N_{coils_{C2}}Area_{rect_{C2}})$$

Where:

- $N_{coils_{BD}} = 100$
- $N_{coils_{C2}} = 500$
- $Area_{trap_{BD}} = 5\frac{(10+20)}{2} = 75mm^2$
- $Area_{rect_{BD}} = 20Z_{B/D}mm^2$
- $Area_{rect_{C2}} = 40Z_{C2}mm^2$

So for the total area to be 0, we need:

$$\begin{aligned} &100 \times (4 \times 75 + 2 \times 20Z_{B/D}) - 500 \times 40Z_{C2} = 0 \\ &30000 + 4000Z_{B/D} - 20000Z_{C2} = 0 \\ &Z_{C2} = \frac{Z_{B/D}+7.5}{5} \qquad (Z_{B/D} \ \& \ Z_{C2} \ in \ mm) \end{aligned}$$

We therefore have a relationship between $Z_{B/D}$ and Z_{C2}, in a similar way to the relationship we found for system 1. The next step is to find a relationship between $\Delta\Phi_2$ and $Z_{B/D}$. Carrying out the same process as for system 1, we find that there is once again a linear relationship between $\Delta\Phi_2$ and $Z_{B/D}$. Figure 25 shows $\Delta\Phi_2$ plotted against $Z_{B/D}$. Using this plot we find that the relationship between $\Delta\Phi_2$ and $Z_{B/D}$ is:

$$\Delta\Phi_2 = 2.531 \times 10^{-5}Z_{B/D} + 1.898 \times 10^{-7} \qquad (Z_{B/D} \ in \ m) \tag{34}$$

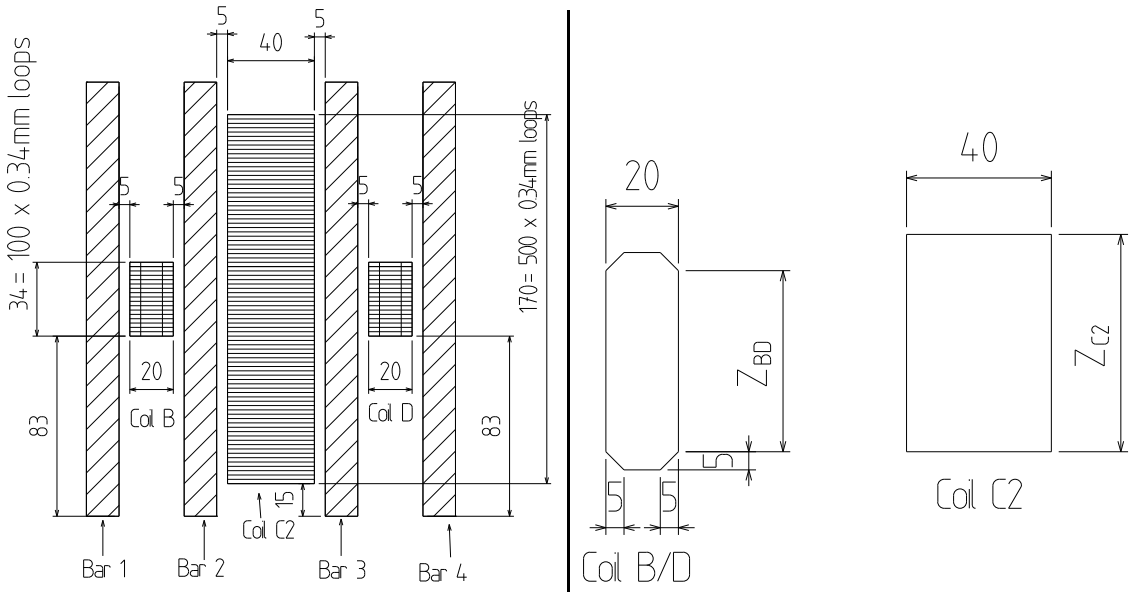

Figure 26: System 2. Left: Front view of the arrangement of probe coils for system 2, coils B and D made up of 100 loops, while coil C2 is made up of 500 loops. Right: Cross sections for the probe coils in system 2, the only variables shall be $Z_{B/D}$ and Z_{C2}. All dimensions in mm.

4.2.3 Combining System 1 and System 2

We have now defined two separate systems, each of which can be varied by just one variable, either $Z_{A/E}$ or $Z_{B/D}$, and both of which fulfil the requirement that the total surface area should be zero. What we now want to do is to combine the two systems, in such a way that the total system sees a magnetic flux which is independent of the distribution of current. Translating this into the variables which we have already defined, what we want is to find a solution such that $\Phi_{total} = 0$, looking at figures 24 and 25 we see that the values of both $\Delta\Phi_1$ & $\Delta\Phi_2$ are positive, thus to get a total of zero we must subtract one system from the other. So what we want is $\Delta\Phi_1 - \Delta\Phi_2 = \Delta\Phi_{total} = 0$. We already have expressions for $\Delta\Phi_1$ & $\Delta\Phi_2$ in terms of $Z_{A/E}$ & $Z_{B/D}$ (equations (33) & (34)), so lets combine them and see what we get:

$$\Delta\Phi_1 - \Delta\Phi_2 = 0$$
$$6.995 \times 10^{-6} Z_{A/E} + 5.02 \times 10^{-8} - 2.531 \times 10^{-5} Z_{B/D} - 1.898 \times 10^{-7} = 0$$

$$\boxed{Z_{B/D} = 0.2764 Z_{A/E} - 0.0055} \qquad (Z_{B/D} \ \& \ Z_{A/E} \ in \ m) \tag{35}$$

What we have therefore is a relationship between the dimensions of system 1 and 2 which will give a total system which sees a flux that is independent of the distribution in the current carrying bars. The next step is to decide upon the dimensions of the system, taking into account real-world considerations for the construction of the probe coils. We don't want probe coils that are either too small or too large, and so I will put a limit on the length of the probe coils such

that no probe coil is longer than $500mm$. Also in order to aid in construction, I will choose dimensions which round the closest to $5mm$ intervals, for example $95mm$ or $60mm$.

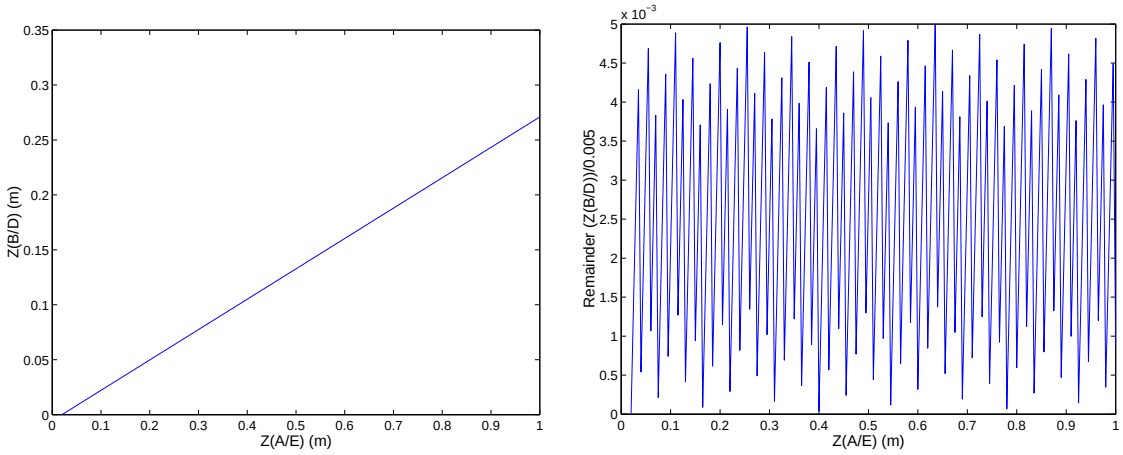

Figure 27: Left: The line on the plot represents the possible pairs of $Z_{A/E}$ and $Z_{B/D}$ given by equation (35). Right: Plot of remainder of $\frac{Z_{B/D}}{0.005}$ against $Z_{A/E}$, the closer the point is to the zero line, the closer the value of $Z_{B/D}$ is to a 5mm interval.

Figure 27 shows the possible values for $Z_{A/E}$ & $Z_{B/D}$, this figure also shows the remainder of $\frac{Z_{B/D}}{0.005}$plotted against $Z_{A/E}$, what we see is that the value of $Z_{B/D}$ appears to be closest to a 5mm interval when $Z_{A/E}$ is $0.4m$ or $400mm$. Using equation (35) we find that this corresponds to a value of $Z_{B/D} = 105mm$. Therefore we have finally arrived at the dimensions of a suitable system to solve our problem, now we have $Z_{A/E}$ & $Z_{B/D}$, the relationships derived previously in this section can be used to find all of the other dimensions. Using these equations we arrive at the following major dimensions:

- $Z_{A/E} = 400mm$
- $Z_{B/D} = 105mm$
- $Z_{C1} = 392.5mm$
- $Z_{C2} = 22.5mm$

We still need to incorporate probe coil C1 and C2 into the same probe coil C, but with the way we have carried out the calculations this should not be a problem. The trapezium sections are not included in the dimensions Z_{C1} & Z_{C2} and so the symmetry of the problem does in fact allow us to simply subtract[24] Z_{C2} from Z_{C1}. Therefore $Z_C = 370mm$, and the trapezium sections for probe coil C will be the same as those for probe coil C1.

Now that we have designed our system, all that remains is to test it and see if it actually gives the results we are looking for. Using the same conventions as previously for the magnetic

[24]The two systems were modeled assuming C1 and C2 had surface vectors pointing in the same direction, so if the total system will be system 1 minus system 2 then we must subtract Z_{C2} from Z_{C1}.

inductances, the total flux seen by the system will be described by the following equation:

$$\begin{aligned}\Phi_{total} = \quad & M_{A1}I_1 + M_{A2}I_2 + M_{A3}I_3 + M_{A4}I_4 \\ & -M_{B1}I_1 - M_{B2}I_2 - M_{B3}I_3 - M_{B4}I_4 \\ & -M_{C1}I_1 - M_{C2}I_2 - M_{C3}I_3 - M_{C4}I_4 \\ & -M_{D1}I_1 - M_{D2}I_2 - M_{D3}I_3 - M_{D4}I_4 \\ & +M_{E1}I_1 + M_{E2}I_2 + M_{E3}I_3 + M_{E4}I_4\end{aligned} \tag{36}$$

Where the mutual inductances are as follows:

M_{A1}:	-1.0390×10^{-5}	M_{A2}:	-7.3000×10^{-6}	M_{A3}:	-4.9493×10^{-6}	M_{A4}:	-3.9936×10^{-6}
M_{B1}:	6.0686×10^{-7}	M_{B2}:	-6.0686×10^{-7}	M_{B3}:	-3.8282×10^{-7}	M_{B4}:	-2.9058×10^{-7}
M_{C1}:	1.2942×10^{-5}	M_{C2}:	1.8110×10^{-5}	M_{C3}:	-1.9110×10^{-5}	M_{C4}:	-1.2942×10^{-5}
M_{D1}:	2.9058×10^{-7}	M_{D2}:	3.8282×10^{-7}	M_{D3}:	6.0686×10^{-7}	M_{D4}:	-6.0686×10^{-7}
M_{E1}:	3.9936×10^{-6}	M_{E2}:	4.9493×10^{-6}	M_{E3}:	7.3000×10^{-6}	M_{E4}:	1.0390×10^{-5}

Table 6: The mutual inductances of the proposed system (In Henrys).

What we want is a system such that:

$$\begin{aligned}\Phi_{total} &= A(I_1 + I_2 - I_3 - I_4) \\ \Phi_{total} &= AI_1 + AI_2 - AI_3 - AI_4\end{aligned}$$

which, from equation (36), gives us:

$$\begin{aligned}M_{A1} - M_{B1} - M_{C1} - M_{D1} + M_{E1} &= A \\ M_{A2} - M_{B2} - M_{C2} - M_{D2} + M_{E2} &= A \\ M_{A3} - M_{B3} - M_{C3} - M_{D3} + M_{E3} &= -A \\ M_{A4} - M_{B4} - M_{C4} - M_{D4} + M_{E4} &= -A\end{aligned}$$

i.e. the contribution to the flux from each of the currents should be equal. If we use the mutual inductance values from table 6, then we find the following:

$$\begin{aligned}M_{A1} - M_{B1} - M_{C1} - M_{D1} + M_{E1} &= -2.0236 \times 10^{-5} = A \\ M_{A2} - M_{B2} - M_{C2} - M_{D2} + M_{E2} &= -2.0236 \times 10^{-5} = A \\ M_{A3} - M_{B3} - M_{C3} - M_{D3} + M_{E3} &= 2.0236 \times 10^{-5} = -A \\ M_{A4} - M_{B4} - M_{C4} - M_{D4} + M_{E4} &= 2.0236 \times 10^{-5} = -A\end{aligned}$$

This certainly seems to fill our original specifications, if we take a look at figure 28 this shows the flux plotted against I_1, with $I_{left} = -I_{right} = 60,000 Amps$. The plot is on the same scale as figure 21 in order to best show the improvement compared to the current system. $\Delta\Phi_{current}$ in the current system is 1.4229×10^{-6}, whereas the $\Delta\Phi_{prop}$ for the proposed new system is 1.0205×10^{-9}, over a thousand times smaller than the current system. This small residual gradient can be attributed to many sources, including the rounding of dimensions to improve constructibility and the fineness of the mesh used to calculate the magnetic field. A fuller investigation into the source of this small residual gradient could be carried out, but would not really add anything new to the work done here.

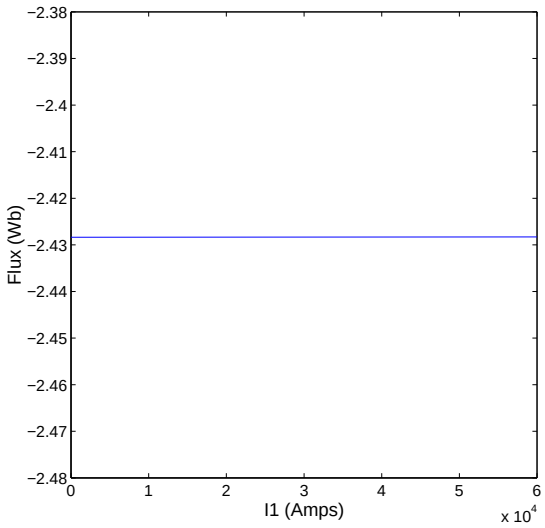

Figure 28: Plot of flux against I_1 for the proposed system of probe coils, with $I_{left} = -I_{right} = 60,000 Amps$

5 Design and Construction Considerations

We now need to used the dimensions calculated using the computer model to design a real system which shall be constructed and installed. We therefore need to take into account real world design considerations. The following section contains detailed plans, with annotation, for the design of each of the new probe coils.

The coils shall all be constructed by winding coils of $0.3mm$ transformer wire, with a packing width of $0.34mm$, onto shaped plastic cores. Once the probe coils have been calibrated, the wire will be coated with a resin to fix it in place. A sheet of copper shall then be wrapped around the whole coil and connected to ground, this will stop any electrical fields from entering the probe coil and causing interference. Finally each coil will be fitted with a plastic case to isolate it electrically from the current carrying bars, an important consideration, as the bars carry around 30,000 Amps each. All parts other than the transformer wire and copper sheet shall be constructed from plastic, including the screws, this is important for two reasons, firstly to stop any interference from magnetic materials, and secondly because of the huge currents passing through the current carrying bars.

The probe coils will then be fixed to plastic boards between the current carrying bars, they will be fixed in place with long plastic screws to ensure that the probe coils are correctly arranged with respect to the current carrying bars. The wires which leave the probe coils will be twisted together to ensure that they do not create further areas for the flux to pass through, which would cause interference with the signal. The following sections contain detailed schematics for each of the probe coils.

5.1 Coils A & E

These two identical coils shall be placed at either side of the system of current carrying bars.

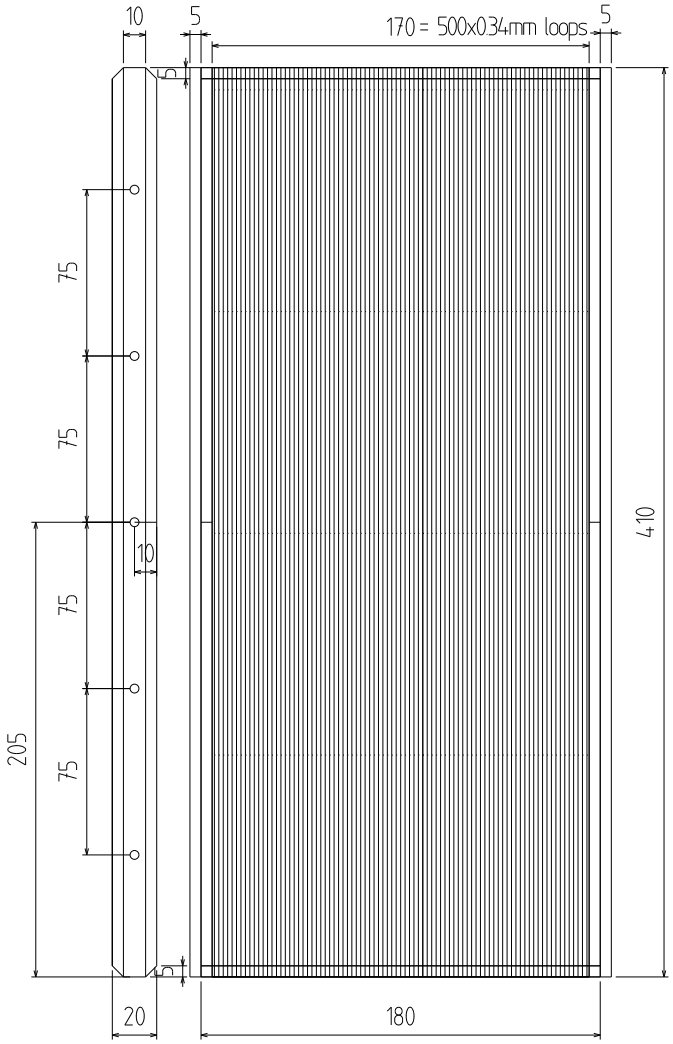

Figure 29: Coil A/E main section, showing the dimensions of the plastic core and the wire loops, as well as the screw holes for fixing the probe coils together. Two of these coils shall be constructed, all measurements in mm.

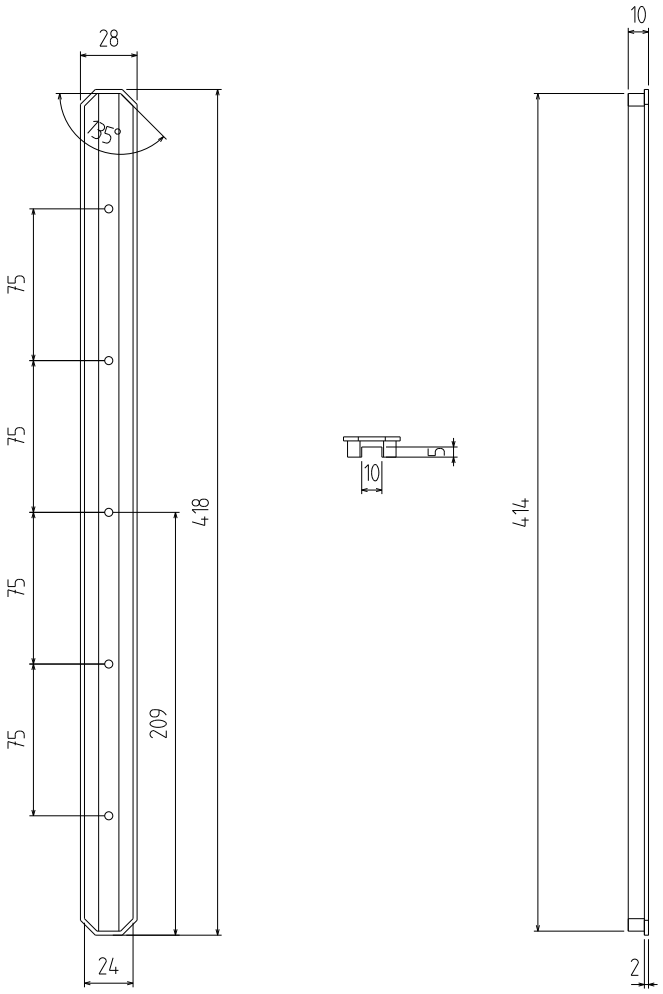

Figure 30: Top and bottom pieces for the probe coils A & E, this pieces fit onto the top and bottom of the probe coils, giving them the form of a capital I. They are there to allow the fitting of a plastic case around the probe coil, and also to make the probe coils sturdier. Four of these pieces will be constructed, all measurements in mm.

5.2 Coils B & D

These two identical coils shall be placed between bars 1 & 2, and bars 3 & 4.

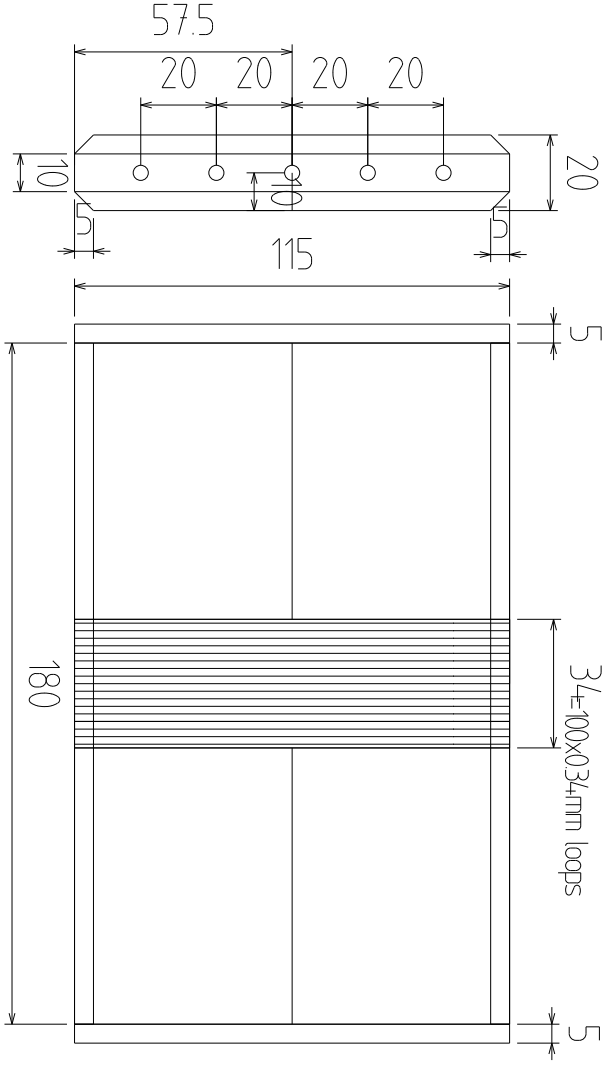

Figure 31: Coil B/D main section, showing the dimensions of the plastic core and the wire loops, as well as the screw holes for fixing the probe coils together. Two of these coils shall be constructed, all measurements in *mm*.

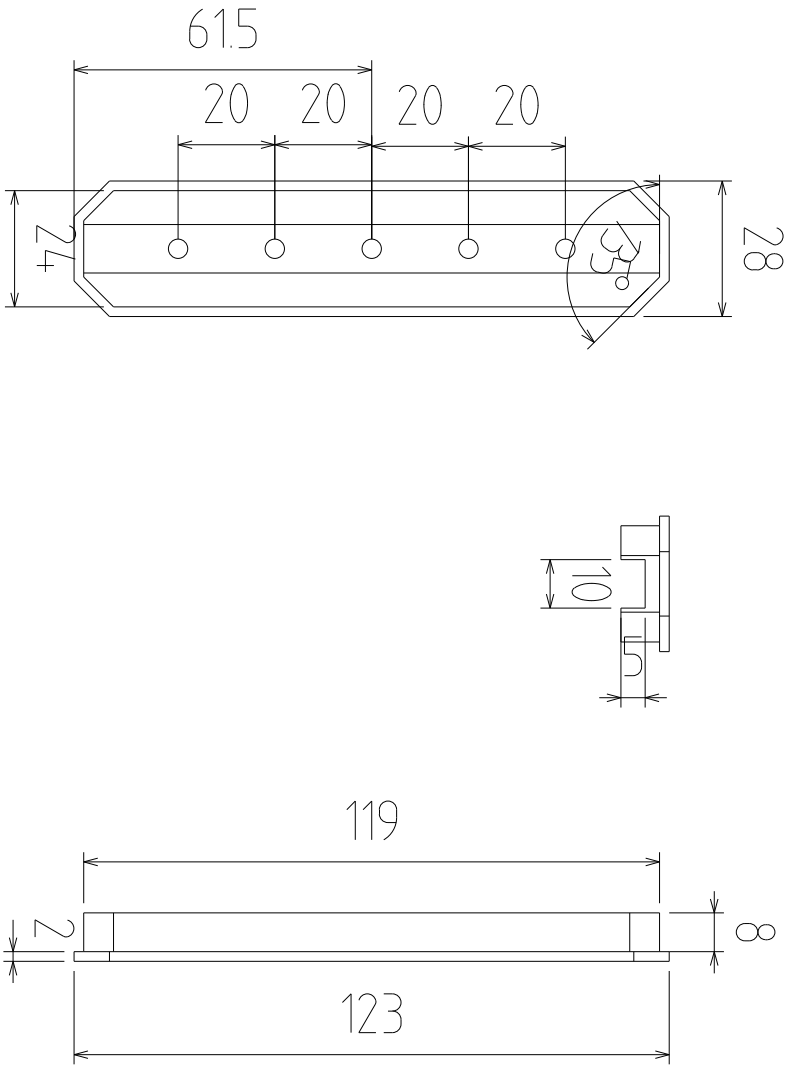

Figure 32: Top and bottom pieces for the probe coils B & D, these pieces fit onto the top and bottom of the probe coils, giving them the form of a capital I. They are there to allow the fitting of a plastic case around the probe coil, and also to make the probe coils sturdier. Four of these pieces shall be constructed, all measurements in mm.

5.3 Coil C

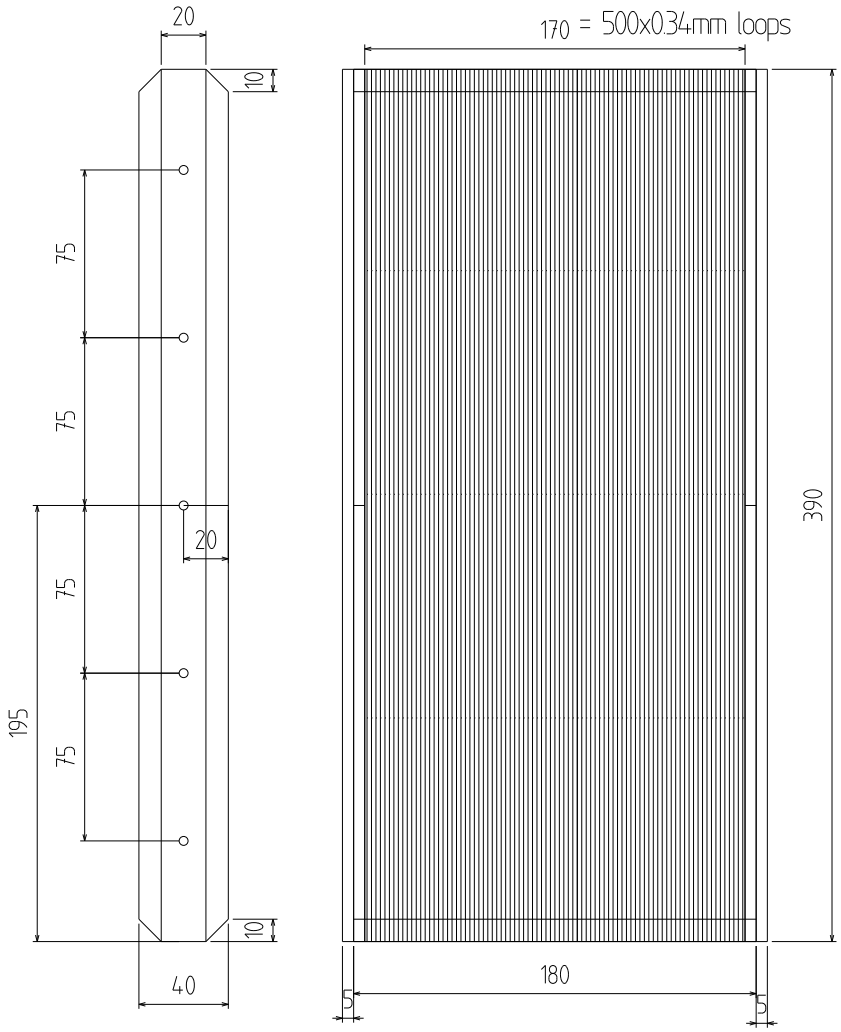

Figure 33: Coil C main section, showing the dimensions of the plastic core and the wire loops. One of these probe coils shall be constructed, all measurements in mm.

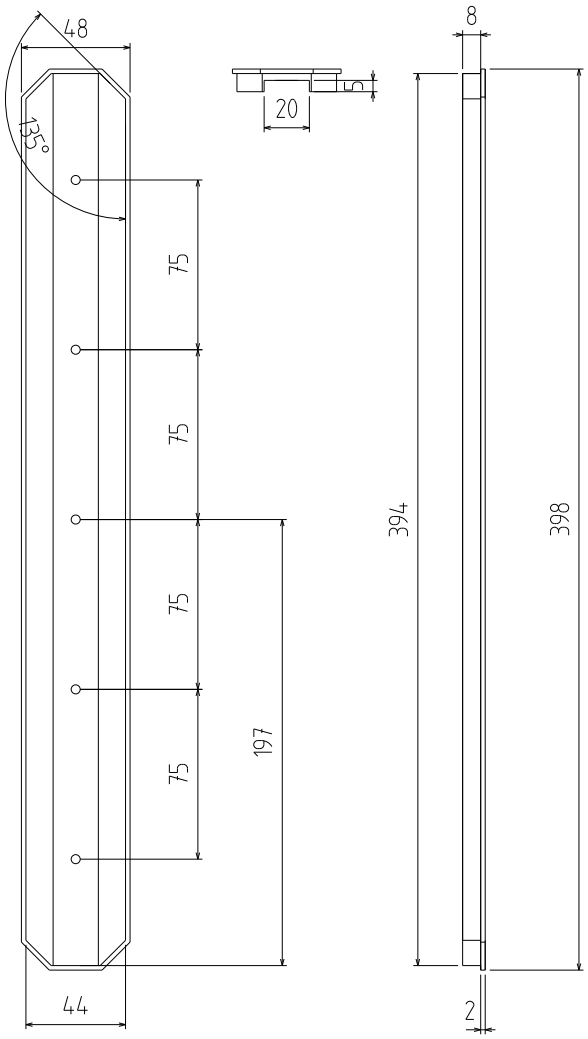

Figure 34: Coil C top and bottom sections, two of these pieces shall be constructed, all measurements in *mm*.

5.4 Arrangement of Probe Coils between Current Carrying Bars

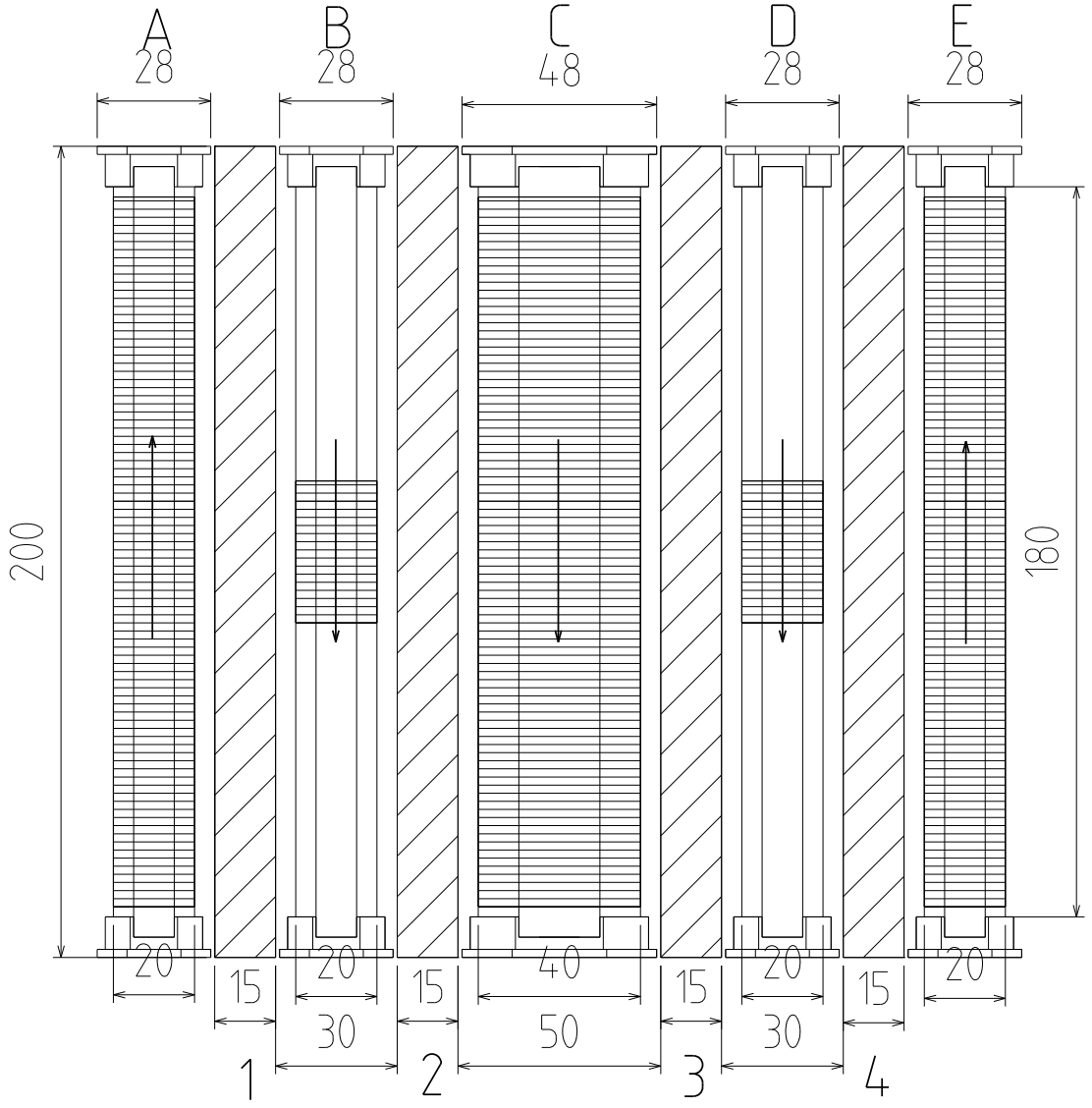

Figure 35: Arrangement of the probe coils between the current carrying bars

Figure 35 shows the arrangement of the five probe coils with respect to the current carrying bars. It is very important that the probe coils are arranged in this way, as the mutual inductance of each coil is affected by its position. The arrows on the probe coils show the way in which they should be connected. I have assumed that all of the probe coils have been wound in the same sense, in other words that the surface vector points in the same direction for each of the probe coils as arranged here. If this is the case then the arrows show in which direction the coils should be connected relative to each other, for example the top connection of coil A should be connected to the top connection of coil B and so on.

6 Discussion of Errors

First a note on errors, since there has been no use of experimental data within this report, it is therefore quite impossible to calculate experimental errors. All of the work carried out here has been done using computer models based on mathematical equations which describe the physical systems in question. The values calculated are therefore exact for the modeled system, and the only source of errors would be those of MATLAB itself, which are small enough to be neglected. This does not however mean that the model is fully representative of the real-world situation, and that the system would function exactly as specified herein. The model used within this paper is fairly basic, and does not take into account the magnetic properties of the materials, or those of surrounding equipment. This however is outside of the scope of the work carried out here, though it may factor into the installation and calibration of the system.

7 Conclusion

The aim of this project was to design a system of probe coils to be arranged around the four current carrying bars which supply current to the toroidal field coils. The new system of probe coils should see a total magnetic flux which is directly proportional to the current, I_t, flowing in the toroidal field coils. A system had already been installed in an attempt to fulfil the above requirements, but the system was flawed as it was based on the assumption that the current would be evenly distributed between the bars. However, this is not the case during the ramping up and down of the current, as the changing current induces a magnetic field which affects the current distribution. This results in the currently installed system seeing different distributions of the same current as different currents.

The model which we constructed in this project takes into account the difference in the distribution of current between the bars. To start with, a model of the magnetic field produced by the current carrying bars was created using MATLAB. After rigorous testing, the model was found to be sound, and suitable for use in this project. The next step was to create model of the probe coils themselves, while taking into account real-world considerations such as the shape and dimensions of the probe coils. This model was then tested and found to perform as expected.

In order to investigate the problem with the currently installed system, made up of three probe coils, it was modeled in MATLAB using the probe coil model discussed above. Using this model we found that there was a linear relationship between the flux seen by the arrangement of probe coils and the distribution of current between the bars.It should therefore be possible to compensate for this problem by adding in a second system, which also has a linear relationship between the flux and the current distribution, but with an opposite gradient.

First a model was created for a system of three probe coils arranged in the same way as the currently installed system. The model was created in such a way that its dimensions could be represented using only one variable. A relationship was found between this variable and the gradient of the equation linking the flux with the current distribution. The same process was then carried out for a second system of three probe coils. It was then a simple matter of solving these two equations, such that the second gradient was the negative of the first, giving

an equation linking the dimensional variables of the two systems. This equation was then used to find the dimensions of a set of probe coils which would fulfil the requirements of our project.

Having a better measurement of the current in the toroidal field coils is an important point, as it will improve the measurement of the plasma pressure by improving the diamagnetic measurement of the toroidal magnetic flux created by the plasma. A better knowledge of the plasma pressure will enable the feedback systems in the TCV to function more effectively, improving the containment and therefore the stability of the plasma. Therefore the work done here has implications for the running of the TCV.

The designed system satisfies the conditions laid out at the beginning of this project, that the flux which threads the system should be independent of the distribution of current between the bars, and also should not be affected by external magnetic fields. I am therefore satisfied that the solution has met all of the original aims of the project. Further work will be needed though, as the coils still need to be constructed, installed, and finally calibrated before being connected to the TCV control systems. The most important of these steps will be the calibration, once installed the probe coils must be frequency calibrated in order to properly take into account the surrounding metallic structures. A lot remains to be done on this system, but once up and running it should provide much improved measurements of the current in the toroidal field coils.

8 A Note on the Work Carried Out in this Project

The following sections of work were carried out by Robert Tye:

- The design, creation and testing of all MATLAB models used in this paper, including the magnetic field models and the magnetic probe coil models.
- The modeling of a new system of probe coils to solve the initial problem, and the derivation of the appropriate dimensions.
- The schematics of the new system.

The mathematical description of the magnetic field of a current carrying bar, described by equations (13) and (14) was taken from [1].

9 Acknowledgements

I would like to thank Dr. Jean-Marc Moret for agreeing to supervise my project, and for aiding me in the understanding of my work. I would also like to thank Anne Le Drian, for being very helpful and supportive in the writing of my report.

References

[1] Heinz E.Knoepfel. *Magnetic Fields: A Comprehensive Theoretical Treatise for Practical Use.* John Wiley & Sons, Inc., first edition, 2000.

[2] M. O. Hagler and M. Kristiansen. *An Introduction to Controlled Thermonuclear Fusion.* Lexington Books, first edition, 1977.

[3] R. F. Heeter, A. F. Fasoli, S. Ali-Arshad, and J.-M. Moret. Fast magnetic fluctuation diagnostics for alfvén eigenmode and magnetohydrodynamics studies at the joint european torus. *Rev. Sci. Instrum.*, 71:4092, 2000.

[4] Richard H. Huddlestone and Stanley L. Leonard. *Plasma Diagnostic Techniques.* Academic Press Inc. (London) Ltd., first edition, 1965.

[5] Adriano Livio MANINI. *Analysis and Interpretation of the Plasma Dynamic Response to Additional Heating Power Using Different Diagnostics.* PhD thesis, EPFL, 2002.

[6] J.-M. Moret, F. Buhlmann, D. Fasel, F. Hofmann, and G. Tonetti. Magnetic measurements on the tcv tokamak. *Rev. Sci. Instrum.*, 69:2333, 1998.

[7] J.-M. Moret, F. Buhlmann, and G. Tonetti. Fast single loop diamagnetic measurements on the tcv tokamak. *Rev. Sci. Instrum.*, 74:4634, 2003.

[8] Hugh D. Young and Roger A. Freeman. *University Physics.* Addison-Wesley, tenth edition, 2000.